Toward Global Soil Moisture Monitoring with Sentinel-1: Harnessing Assets and Overcoming Obstacles

Bernhard Bauer-Marschallinger, *Member, IEEE*, Vahid Freeman, Senmao Cao, Christoph Paulik, Stefan Schaufler, Tobias Stachl, Sara Modanesi, Christian Massari, Luca Ciabatta, Luca Brocca, Wolfgang Wagner, *Senior Member, IEEE*

***Abstract*—Soil moisture is a key environmental variable, important to e.g. farmers, meteorologists, and disaster management units. Here, we present a method to retrieve Surface Soil Moisture (SSM) from the Sentinel-1 satellites, which carry C-band Synthetic Aperture Radar (S-1 CSAR) sensors that provide the richest freely available SAR data source so far, unprecedented in accuracy and coverage. Our SSM retrieval method, adapting well-established change detection algorithms, builds the first globally deployable soil moisture observation dataset with 1km resolution.**

The paper provides an algorithm formulation to be operated in data cube architectures and High Performance Computing (HPC) environments. It includes the novel Dynamic Gaussian Upscaling (DGU) method for spatial upscaling of SAR imagery, harnessing its field-scale information and successfully mitigating effects from the SAR's high signal complexity. Also, a new regression-based approach for estimating the radar slope is defined, coping with Sentinel-1's inhomogeneity in spatial coverage.

We employ the S-1 SSM algorithm on a 3yr S-1 data cube over Italy, obtaining a consistent set of model parameters and product masks, unperturbed by coverage discontinuities. An evaluation of therefrom generated S-1 SSM data, involving a 1km Soil Water Balance Model (SWBM) over Umbria, yields high agreement over plains and agricultural areas, with low agreement over forests and strong topography. While positive biases during the growing season are detected, excellent capability to capture small-scale soil moisture changes as from rainfall or irrigation is evident.

The S-1 SSM is currently in preparation towards operational product dissemination in the Copernicus Global Land Service (CGLS).

***Index Terms*—Soil Moisture, Change Detection Algorithms, Image Sampling, Sentinel-1, Copernicus.**

B. Bauer-Marschallinger, V. Freeman, S. Cao, C. Paulik, T. Stachl, and W. Wagner are with the Department of Geodesy and Geoinformation, Vienna University of Technology (TU Wien), 1040 Vienna, Austria (e-mail: bernhard.bauer-marschallinger@geo.tuwien.ac.at; vahid.freeman@geo.tuwien.ac.at; senmao.cao@geo.tuwien.ac.at; christoph.paulik@geo.tuwien.ac.at; stefan.schaufler@geo.tuwien.ac.at; tobias.stachl@geo.tuwien.ac.at; wolfgang.wagner@geo.tuwien.ac.at).

S. Modanesi, C. Massari, L. Ciabatta, and L. Brocca are with the Research Institute for Geo-Hydrological Protection, National Research Council, Perugia 06128, Italy (e-mail: sara_m85@libero.it; c.massari@irpi.cnr.it; l.ciabatta@irpi.cnr.it; luca.brocca@irpi.cnr.it)

I. Introduction

THE SENTINEL-1 SATELLITES have been scanning the Earth's surface using high-resolution radar sensors since 2014 with unprecedented spatio-temporal coverage. They carry a Synthetic Aperture Radar system (SAR) and deliver information on surface properties independent from daylight and cloud cover, operating in C-band (5.405 GHz). It is a mission of the European earth observation program *Copernicus* with two identical spacecrafts, Sentinel-1A (S-1A) launched in April 2014 and Sentinel-1B (S-1B) in April 2016. Together with the multi-spectral sensors of the Copernicus constellation onboard Sentinel-2 [1] and Sentinel-3 [2], the Sentinel-1 SAR mission [3] is a pillar of current and future Earth observation.

High expectations have been raised by the Sentinel-1 mission. The two Sentinel-1 satellites share the same orbit 180° apart and follow a strict acquisition scenario with a 12-day repeat cycle, featuring stable viewing angles, and thus predictable viewing geometry and spatial coverage. This setup enables via SAR interferometry the detection of millimetre-scale vertical surface deformations within 6 days. In its main sensing mode over land, the Interferometric Wide Swath Mode (IW), the Sentinel-1 SAR offers a Ground Range Detected (GRD) resolution of 20m×22m at revisit frequency of 1.5-4 days over Europe (sensed from different orbits).

However, the sensor design and acquisition strategy constitutes also a break with the antecedent C-band SAR missions ERS-1/2, Envisat ASAR and Radarsat-1/2, as it provides HH-polarised observations only over polar areas and limits the range of observations angles. Having said that, its spatio-temporal resolution is outstanding as it surpasses the level of detail of its predecessor missions ERS-1/2 and Envisat ASAR, or any other civil microwave missions, by far. In conjunction with the anticipated radiometric accuracy and stability, its projected longevity, and its free-data-policy, the Sentinel-1 radar mission has drawn much attention in the remote sensing community as well as among users.

One major application of Sentinel-1 is soil moisture monitoring. Knowledge on soil moisture is essential for the assessment of the global water-, energy- and carbon- cycles [4]. Surface Soil Moisture (SSM), defined as the water content of the top few centimetres soil, is a key driver of water and heat fluxes between the ground and the atmosphere, altering air temperature and humidity [5]. Vice versa, it is

very sensitive to external forcing in form of precipitation, temperature, solar irradiation, humidity and wind. SSM is thus both an integrator of climatic conditions [6] and a driver of local weather and climate [7]. Consequently, the knowledge of the spatial and temporal variation of SSM is crucial in the fields of meteorology, climatology, hydrology, and agronomy. More specifically, estimation of soil moisture can be a critical skill in numerical weather prediction [8]–[10], precipitation estimation [11], [12], flood risk modelling [13], [14], runoff prediction [15], groundwater recharge modelling [16], irrigation assessment [17], and creating understanding of heatwaves [18], droughts [19], ocean-land-feedbacks [20], and long-term trends in hydrology [21]. On these grounds, soil moisture is listed as essential climate variable (ECV) within the framework of the Global Climate Observing System [22].

Microwave remote sensing has demonstrated its capability in observing SSM in a globally consistent and comprehensive way, reaching maturity during the last decade [23]. Alternatively, in-situ techniques [24] allow for accurate measurements at point scale, but lack spatial representativeness and require equipment, maintenance and ground access. For areal-extensive or global undertakings, the use of coarse-scale measurements (12-50km) from active (radars) or passive (radiometers) microwave sensors for SSM retrieval is well established and in operational use. Remotely sensed soil moisture data from Metop ASCAT [25], Windsat [26], SMOS [27], SMAP [28] have been thoroughly evaluated and found widespread use [29], [30].

Coarse-scale sensors as exemplified above have a large swath/footprint and can capture temporal soil moisture dynamics well with their daily or sub-daily revisit times. However, they lack spatial details. They do not support analysis of local hydrological patterns below the 10km scale, such as effects from convectional rains or topography and thus do not meet the requirements of many applications. With the aim to enhance the spatial resolution, many different approaches have been developed in order to obtain sub-pixel SSM information. The methods range from geostatistical analysis [31], to data fusion [32], [33], and to upscaling algorithms applying subpixel-patterns [34]–[36]. They have in common the need for auxiliary data, either temporally concurring observations from different bands, or a-priori local data as e.g. knowledge on the local land cover or soil properties, which are commonly not available everywhere nor are of consistent quality. A comprehensive survey on upscaling methods for soil moisture is given by [37].

Contrary, SAR remote sensing systems like the (elapsed) Envisat ASAR and the current Sentinel-1 CSAR radar can directly resolve dynamics at the kilometric scale and below. SAR technology involves advanced radar signal processing, providing sub-antenna footprint resolution by means of range and Doppler discrimination [38]. With this, the sensors deliver high-resolution radar imagery of the Earth's geometric and dielectric properties, potentially resolving objects at the field level, i.e. at the scale of some 10m. Recent studies demonstrated the capability of SAR sensors to map SSM using neural-network-based approaches, employing observations from Envisat ASAR [39], TerraSAR-X [40], and Sentinel-1 [41]. Previously, [42] introduced a change detection method for SSM retrieval from Envisat ASAR HH-polarised data, showing capability to monitor soil moisture dynamics at the continental level and potential for model assimilation [43].

Our proposed SSM retrieval method builds upon this previous work, involving the TU Wien backscatter model and time series analysis. We adopt this model to the new Sentinel-1 sensor, and its alterations are designed to harness the high-resolution IW mode measurements and to extract optimally the kilometric SSM signal, which is in demand among many user groups [44]. The underlying algorithm has to cope with the immanent challenges of the Sentinel-1 SAR data: 1) The high complexity of the SAR signal at field scale, at which the soil moisture signal is superimposed by many scattering signals, and 2) the inhomogeneous spatial coverage of the Sentinel-1 mission due to its acquisition strategy, leading to problems in building consistent backscatter time series necessary for model calibration.

The following section shortly reviews the Sentinel-1 mission- and sensor- characteristics and discusses the novel challenges brought by Sentinel-1 in detail. This is followed by a methods section about the proposed adaption of the SSM retrieval algorithm. Subsequently, results from a evaluation campaign of the obtained 1km Sentinel-1 SSM data over Umbria in Italy is presented and discussed. The article closes with an outlook on upcoming improvements.

II. A New Sensor for SSM: Sentinel-1 CSAR

The European SAR missions ERS-1/2 (launched 1991) and Envisat ASAR (launched 2002) trailblazed the SAR technology in Earth observation. The Sentinel-1 mission (launched 2014) builds on this heritage and institutes the first operational SAR global monitoring system, providing open data with unprecedented quality, accuracy and spatio-temporal coverage.

Sentinel-1A and Sentinel-1B form the first satellite pair and observe the Earth operationally since October 2014 and October 2016, respectively. Each spacecraft has a foreseen life time of 7 years, with consumables on-board allowing an extension up to 12 years. Mission continuity is assured as the follow-up satellite pair Sentinel-1C and -1D will extend the operational monitoring component at least until the end of 2030[1].

A. Specifications for Land Applications

The Sentinel-1 satellites carry a C-band SAR instrument (CSAR) operating at a centre frequency of 5.405 GHz with support for co- and cross-polarisation receive channels, potentially operating at four exclusive acquisition modes. While three modes focus on maritime and emergency operations, the Interferometric Wide swath (IW) mode is the main acquisition mode over (non-polar) land, designed to satisfy the majority of user requirements [45].

In IW mode, CSAR acquires data with a 250 km swath, spanning an incidence angle range over flat terrain from 29.1°

[1]http://www.esa.int/Our_Activities/Observing_the_Earth/Copernicus/Sentinel-1/Deal_sealed_for_new_Sentinel-1_satellites

to 46.0°. More specifically, it captures and merges consecutively three parallel sub-swaths using the TOPSAR (Terrain Observation with Progressive Scans SAR) imaging technique [46]. At single look, its spatial resolution is 5m×20m, yielding after multi-looking a ground-range-detected resolution 20m×22m in the high-resolution product (IWGRDH). The radiometric accuracy is specified with 1dB (3σ).

Prior to the launch of Sentinel-1A, dedicated studies on the potential for global SSM monitoring were carried out [47]–[49]. They agree that through the mission's design, the Sentinel-1 constellation is a suitable system for operational soil moisture services. It enables global monitoring in a regular manner and thanks to the long planned mission life time, it lays the foundation for long and consistent time series. On these matters, it achieves capabilities comparable to operational meteorological missions as e.g. Metop ASCAT. However, by contrast, Sentinel-1 resolves ground features with a spatial sampling of 10m and at a high radiometric accuracy and thus allows for the retrieval of hydrological signals at much more spatial detail. With SAR information at this scale, effects from land cover, vegetation, topography and also small-scaled hydrological phenomena like convectional rains or floods may be described, which are not seen by coarse-scale systems. Concerning temporal resolution, the Sentinel-1 does not reach the frequency of meteorological systems, but still improves much against preceding SAR missions.

B. From a complex SAR signal to SSM dynamics

Despite its favourable sensor characteristics, the direct exploitation of high-resolution SAR data for SSM retrieval is complicated by several matters. One issue is that small-scaled contributions to the radar backscatter from individual ground features may obscure the soil moisture signal, rendering common algorithms incapable of SSM retrieval at this scale [50], [51]. Furthermore, the influence of soil roughness and vegetation dynamics on the radar signal and the penetration depth is less understood than in the coarse-scale case [41], leading to biases during the vegetation period.

We elaborate on these issues with an example SAR image in Figure 1, showing an Sentinel-1 IWGRDH image from a section of the Danube river in western Hungary. It illustrates the high degree of complexity of SAR backscatter over land at field scale, which is understood in our context as the scale of 10m sampling (equivalent to 20m resolution). In the image, distinct objects like waterbodies, roads, buildings can be easily resolved, also agricultural fields are differentiated, each with a individual SAR response as a conglomerate of local crop and soil status. Yet, the signal is sensitive to many individual, highly-variable features. Concerning vegetation, these include water content, crop row orientation, size, density, even wind bending; concerning soil, these include roughness, tillage and moisture. Disentangling those signals is scientifically challenging [44], [52], [53] and furthermore, it is hardly automatised and thus troubling operational dissemination.

One approach to mitigate this problem is to upscale the SAR signal to the kilometric scale. When done correctly, the SAR signal at a 500m sampling holds the kilometric-scale soil moisture signal, while underlying signals at field-scale driven by roughness, vegetation and penetration depth are minimised. Two assumptions are made here: 1) A region's individual fields and zones are subject to persistent regional soil moisture patterns and thus show alike soil moisture dynamics. This is supported by the temporal stability concept [54], suggesting that a local soil moisture signal is highly correlated with the regional soil moisture signal from the larger surrounding area. 2) Roughness-driven signals induced by soil- and plant-structure of individual fields and zones are mutually independent and thus sum up incoherently during spatial averaging [38]. In practice, this holds on the condition that cultivated areas at the regional scale are not completely well-aligned, nor subject to coherent tillage patterns, otherwise leading to azimuthal effects [55].

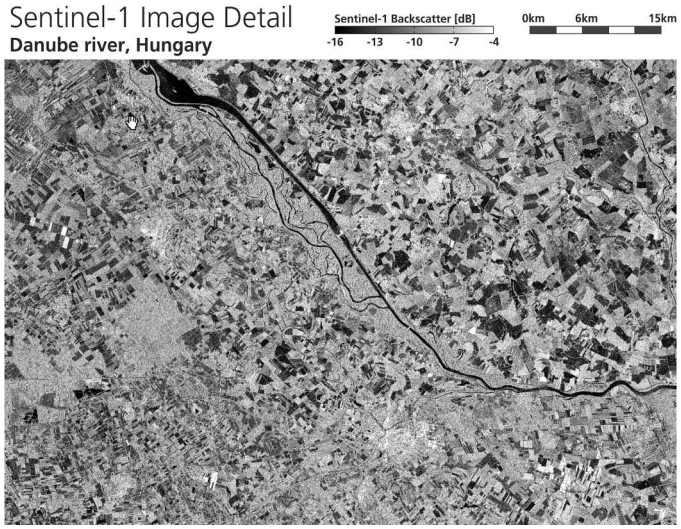

Fig. 1. A detail scene of a Sentinel-1 IWGRDH image at a section of the Danube river in Hungary, measured in VV-polarisation from orbit Nr. 124 on 2016-05-24 at 05:01.

A technique suitable for radar image upscaling is outlined in [56], a work pioneering in image pyramid generation. Here, each level of an image pyramid holds a upscaled representation of its parent level image and results from low-pass filtering and subsequent value aggregation, reducing concordantly the sample size and spatial frequency. Practically, the reduced image may be calculated by convolving the input image with a Gaussian kernel and subsequent local averaging.

Notwithstanding the substantial downsampling from 10m to 500m, the original field-scale backscatter signal can be very useful in such an approach, helping to remove effects of processes different than soil moisture variations. Very high backscatter-values originate most likely from cities and other man-made objects that act as corner reflectors. Very low backscatter-values mainly originate from standing water surfaces. Accordingly, extreme backscatter measurements are highly unlikely to carry any soil moisture signal and they can be discarded from further SAR to SSM processing. This thresholding & discarding can be applied to each Sentinel-1 input image individually and is here referred to as dynamic masking.

On this account, a specialised resampling algorithm that combines upscaling and dynamic masking can skilfully transform the high-resolution information of the Sentinel-1 SAR signal from a 10m to a 500m sampling. A thereof retrieved 1km SSM product eventually describes the soil moisture dynamics at medium scale with high quality, effectively reducing the inherent uncertainties from roughness variability and non-soil surfaces. Having said this, the SAR backscatter model still needs to account for the signal dynamics induced by seasonal changes in the vegetation density at the 1km scale.

C. Effects from the Acquisition Strategy

The Sentinel-1 mission is based on a constellation of two identical satellites in the same orbital plane. The spacecrafts follow a near-polar sun-synchronous orbit at 693km mean altitude and a mean local solar time 18h at ascending node and 6h at descending node. As interferometry requires stringent control of orbit and viewing direction, the spacecraft positions are maintained within an orbital tube of 50m (1σ) [3].

The temporal revisit time is the time between two overpasses of one particular ground location from the same orbit location, repeating the exact acquisition geometry. This is for one Sentinel-1 satellite exactly 12 days, and for two satellites 6 days. As a consequence from this acquisition strategy, and not anticipated by the feasibility studies in [47]–[49], the spatio-temporal coverage of Sentinel-1 is highly inhomogeneous in two respects:

First, in alignment with the Sentinel High Level Operations Plan (HLOP) [57], the Sentinel-1 acquisition strategy prioritises European landmasses over other regions, as a necessity from the CSAR duty cycle. The CSAR is technically constrained by energy and downlink limitations, and is capable of sensing in IW mode to a maximum of only 25 out of 99 minutes per orbit. The HLOP stipulates to employ the limited capacities with priority over ESA's member- and associate-states. The current global coverage can be seen on daily updated maps in the public data catalogue[2] of the Earth Observation Data Centre (EODC).

Second, the effective ground coverage is not uniform. Ground locations are overpassed differently often by the satellites during the 12 day orbit cycle. This so-called coverage frequency time is in general improving with latitude, but shows also a longitudinal component. The repeating orbit configuration leads to a rhomboid pattern in the ground footprint, resulting in areas of high observation frequency next to areas of low observation frequency. Figure 2 shows the hitherto coverage pattern of Sentinel-1A over Europe for the period Oct 2014 - Oct 2016. It is noteworthy that Sentinel-1B, as with identical orbit configuration as Sentinel-1A, does not mitigate the spatial differences. However, the local coverage frequency is then improved by the factor 2 and gives a temporal resolution (the coverage frequency) of 1.5 to 4 days over Europe.

Another consequence of the stringent spacecraft vectors and the repeating orbit setup is the already mentioned stability of the acquisition geometry across orbit cycles. Accordingly, an individual ground location is observed from a finite number of so-called local incidence angles (LIA). Directly related to the ground coverage pattern, this number ranges from 2 LIAs at the equator, to 6 LIAs at the poles (with descending and ascending azimuth aspects), and also follows the rhomboid pattern, yielding sections with more LIAs next to sections with less.

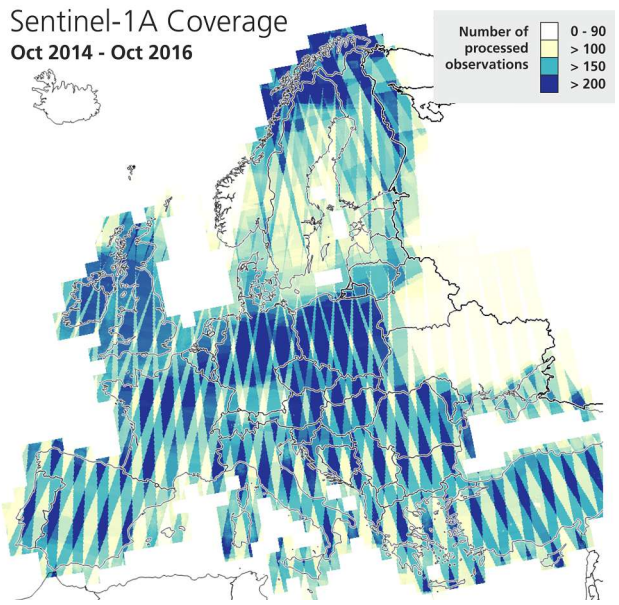

Fig. 2. Sentinel-1A coverage pattern: Number of observations per location over Europe in the first two mission years. Observations from later periods and from Sentinel-1B are not included due to uncompleted processing status.

Overall, the regular acquisition scheme facilitates consistent and predictable observations and is a feature not implemented in older SAR missions. The stable orbit geometry may be advantageous for interferometry and other applications, but for SSM retrieval it poses new challenges: 1) The temporal quality of the SAR signal varies much, with a persistent geographical pattern, favouring some zones over adjacent zones. Hence, the SSM signal quality will not be consistent over space. As a subsequent consequence, the parameter for SSM retrieval, which are built from the SAR time series, will reach maturity in unfavoured areas later. This applies also for non-European areas, where the measurement frequency is in general lower. 2) It leaves some areas with a narrow LIA-range, where the viewing angle dependency of the SAR backscatter cannot be determined, and thus observations from different viewing geometries cannot be directly compared or combined. This relation of backscatter to LIA is commonly refereed as backscatter slope and was essential to previous SSM retrieval algorithms [42], [58].

Apart from geographic issues, stipulations in the Sentinel HLOP have one further impact on SSM retrieval undertakings. The IW mode is only conflict-free with the other modes when observing in VV+VH polarisation [57]. This entails that land surfaces are mainly observed in VV and VH polarisation, discontinuing HH-polarised observations of (non-polar) land as done by preceding SAR missions. VV-backscatter signals stem not only from the soil but also significantly from vegeta-

[2]https://eomex.eodc.eu/cm

tion body and canopy, as they interact more with the (mostly vertically structured) vegetation than in HH-polarisation [59]. This complicates the isolation of soil moisture dynamics and potentially aggravates seasonal vegetation biases in SSM time series [60].

III. The Sentinel-1 SSM Retrieval

The here presented Sentinel-1 SSM retrieval algorithm is based on the TU Wien Change Detection Model [61], which derives SSM directly from observed radar backscatter, measured as backscatter coefficient σ^0. In this model, changes in backscatter are interpreted as changes in soil moisture, while other surface properties as geometry, roughness and vegetation structure are interpreted as static parameters. The model parameters describe maximum dry- and wet- conditions, as well as average signal contributions from vegetation and surface geometry. The model is self-calibrated at the pixel scale, as the model parameters are estimated through statistical analysis of long-term backscatter time series. For the SSM estimation, the actual backscatter-value $\sigma^0(\theta, t)$ at time t and observation angle θ is normalised to a reference angle Θ and linearly scaled between dry- and wet-reference values, yielding relative surface soil water saturation $SSM(t)$ in percent:

$$SSM(t) = \frac{\Delta\sigma^0(\Theta, t)}{S(\Theta)} \quad [\%] \tag{1}$$

Here, $\Delta\sigma^0(\Theta, t)$ is the change in normalised backscatter (relative to dry conditions), and $S(\Theta)$ is the sensitivity to SSM changes at the reference angle Θ. The sensitivity is equivalent to the local backscatter dynamic range, which is estimated by the difference between the normalised backscatter coefficients at wet- and dry- conditions:

$$S(\Theta) = \sigma^0_{wet}(\Theta) - \sigma^0_{dry}(\Theta) \quad [\mathrm{dB}] \tag{2}$$

The model has proven well its capability to produce reliable soil moisture estimates on a global basis, ingesting C-band backscatter measurements from ERS-1/2 [62], [63], Envisat ASAR [43], [64], and Metop ASCAT [65]–[67], whereas for the latter the model is expanded with a dynamic vegetation correction (which is not implemented in the here presented algorithm).

The adaption to Sentinel-1 builds upon knowledge gained with data acquired from 2004 to 2012 through the Envisat ASAR mission [42], [43], [68], the preparatory study of [48], and hands-on experience gained during the first years of operations [69]. As a result, the novel algorithm complies with the actual specific attributes of the Sentinel-1 sensor- and orbit-configuration. Its design allows to efficiently extract the kilometric SSM-signal from the Sentinel-1's 10m IWGRDH data stream, while mitigating impacts from abovementioned spatio-temporal coverage inconsistencies.

The algorithm's novelty consists of 1) a specialised SAR upscaling procedure involving dynamic masking, 2) a new approach for estimating the slope parameter describing the incidence-angle-dependency, 3) a more stable estimation of dry- and wet-reference parameters, and 4) a new procedure for creating static masks. Moreover, 5) the algorithm is formulated to be operated in data cube architectures, harnessing the processing power of High Performance Computing (HPC) environments. The following sections describe in detail the complete processing of Sentinel-1 backscatter observations to 1km SSM values.

A. Sentinel-1 Data Cube at TU Wien

The preparatory study of [48] examined the volume and timeliness of the Sentinel-1 data stream. With a daily data volume of 1TB, it places high demands on processing- and storage- facilities. It concluded that global-scale services in near-real-time (NRT) or reprocessing activities are technically feasible when employed in HPC environments. With this, a Sentinel-1 product retrieval algorithm is then required to support parallelisation.

In recognition of these findings, the Remote Sensing Group of the TU Wien Department of Geodesy and Geoinformation developed a fully-fledged, parallel-operating, Sentinel-1 processing chain [70] that is built on an optimised data cube architecture [71]. Its basic framework is the Equi7Grid [72], a spatial reference system designed to handle efficiently the archiving, processing and displaying of high resolution raster data over land, while preserving geometric accuracy. It is defined for the entire Earth and consists of seven planar subgrids for each continent, referenced to the ellipsoidal WGS84 datum. The coordinates are defined by individual realisations of the Equidistant Azimuthal projection, given as eastings and northings in metres. The Equi7Grid[3] not only allows to handle conveniently large remote sensing spatio-temporal data, but also to relate and transform data of diverse spatial scales [73].

Naturally, the data cube approach is also well suited for the SSM retrieval, since parallel image operations as well as time series analyses are facilitated. Consequently all processed backscatter- and SSM- data of this study are organised in the Equi7Grid.

B. Preprocessing of Raw Sentinel-1 IWGRDH

The preprocessing of the Sentinel-1 data comprises SAR-geocoding, radiometric correction and spatial resampling, and yield a gridded SAR image database with a 500m sampling.

As initial step, the processor ingests the VV-polarised IW data in GRDH format, which is already-focused SAR intensity data that has been detected, multi-looked and projected to ground range, given as images in ellipsoidal coordinates at optimal sampling of 10m. The geocoding and radiometric correction is done with ESA's Sentinel Application Platform (SNAP[4]). In detail, the Range Doppler Terrain Correction reduces the geometric distortions present in SAR data due to the observation geometry and the topography, employing the fully global 90m SRTM DEM from VFP[5]. The output backscatter images are stacked in the Equi7Grid data cube.

[3]Equi7Grid definitions and tools are available at https://github.com/TUW-GEO/Equi7Grid

[4]SNAP - ESA Sentinel Application Platform v5.0.0, http://step.esa.int

[5]$3''$-voidfilled-SRTM, http://www.viewfinderpanoramas.org/

C. Upscaling to 1km Scale

Next, the SAR upscaling/downsampling to the 1km-scale/500m-sampling is performed. The method is a combination of dynamic masking of SAR-values and image reducing operators and shall be named Dynamic Gaussian Upscaling (DGU), in reference to the Gaussian image pyramid technique. Each SAR image is then upscaled individually as follows:

1) Dynamic masking: Very high and low backscatter measurements are highly unlikely to carry any soil moisture signal and thus are discarded. The thresholds for our C-band Sentinel-1 SAR images in VV-polarisation are set to linear equivalents of -5dB and -20dB, with the the upper limit construed from qualitative comparisons with urban areas from CORINE 2012 land cover [74] and optical imagery from Sentinel-2, and the lower limit conservatively construed from the sensor's Noise Equal Sigma Zero (NESZ) at -22dB. Because the value range in linear domain spreads over many powers of ten, the masking of high values is of chief importance, as those 10m-points are kept from spreading into the 500m-point during the resampling, polluting the output image with non-representative values. Figures 3 exemplifies this effect over a rural area in southwest England, where several artificial structures act as corner reflectors. Especially when they form star-shaped artefacts in the SAR image (a), downsampling is an ill-posed problem at which common methods as the Bilinear Interpolation fail to represent the average local backscatter (b). Through masking out high backscatter pixels before resampling (d), the DGU method effectively removes those artefacts (e).

2) Pixel aggregation: For each target 500m pixel, the contained non-masked 10m pixels (sub-pixels) are averaged to one value by arithmetic mean. The averaging of the values is done in the linear domain in order to correctly add backscatter intensities.

3) Gaussian filtering: To remove aliasing effects generated by the pixel aggregation (as e.g. in Figure 3b), a Gaussian filter $G_{1\mathrm{km}}$ with a Full Width at Half Maximum (FWHM) equal to 1km is applied onto the image. The FWHM, as a means of spatial low-pass cutoff frequency [75], relates to the standard deviation σ of $G_{1\mathrm{km}}$ as:

$$\sigma_{G_{1\mathrm{km}}} = \frac{\mathrm{FWHM}}{\kappa} = \frac{1000}{2\sqrt{2\ln 2}} = 424.7 \quad [\mathrm{m}] \qquad (3)$$

The conversion factor κ stems from the probability density function of the Gaussian distribution. $G_{1\mathrm{km}}$ is a low-pass-filter that suppresses signals with spatial frequencies shorter than 1km, while preserving signals with longer frequencies. Yet, contrary to common resampling tools (e.g. GDAL), the present resampling procedure reduces concordantly an image's sample size and spatial frequencies and thus complies with Nyquist's sampling theorem.

As a note, according to theory (e.g. from [56]), the filtering must be applied before the aggregation when downsampling/upscaling an image. However, the downsampling by factor 50 requires a very large kernel with a size of about 160×160 to represent the $G_{1\mathrm{km}}$ (to cover 95% of the density function), hence the image convolution needs much computation time.

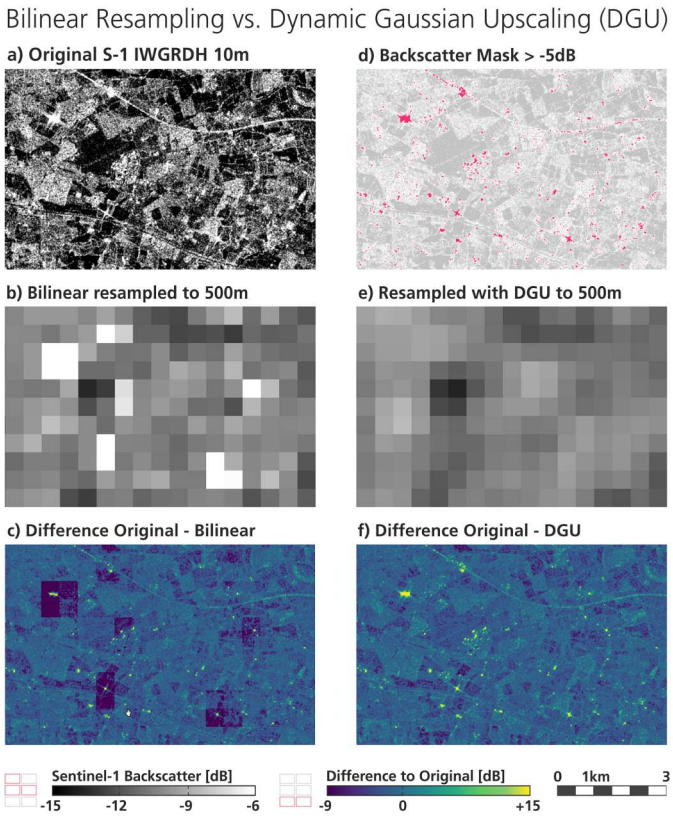

Fig. 3. Resampling of Sentinel-1 SAR backscatter imagery over agricultural area in southwest England, featuring artificial objects with high backscattering coefficient. (a) Original backscatter image. (b) Image resampled to 500m by Bilinear Interpolation (no mask applied), showing polluted pixels, and also aliasing (c) Difference to original 10m-sampled image, highlighting block-shaped artefacts (d) -5dB mask used for dynamic masking. (e) Image resampled to 500m with Dynamic Gaussian Upscaling (DGU) method. (f) as (c), highlighting the accurate removal of strong backscatters.

Alternatively, when the pixel aggregation is done beforehand as suggested here, the convolution[6] is applied on a 500m-sampled image and $G_{1\mathrm{km}}$ can then be approximated by a 3×3 kernel:

$$G_{1\mathrm{km}} = \frac{1}{16}\begin{bmatrix} 1 & 2 & 1 \\ 2 & 4 & 2 \\ 1 & 2 & 1 \end{bmatrix} \qquad (4)$$

4) No-data-value imprinting. Pixels without any backscatter-values, and pixels with less than 1% valid sub-pixels within, are set to the no-data-value. With this, backscatter values from soil surfaces are propagated into adjacent (semi-) urban areas. Pixels dominated by water bodies are masked out in a later step (see Section III-F).

D. Model Parameter Generation

The SSM algorithm requires model parameters for the estimation of relative soil moisture content. These parameters are inferred from the Sentinel-1 backscatter archive through time series analysis. For each grid point, the backscatter time series is built and statistically examined. Therefrom, the (static) parameters are retrieved and saved to disk as parameter

[6]convolve() of astropy v2.0.1, http://www.astropy.org/

layers, holding values on backscatter distribution, observation frequency and incidence angle dependency.

1) SAR Slope and LIA Normalisation: The dependency of the backscatter to the local incidence angle (LIA, θ) is described by the slope parameter β. This can be modelled in the most simple way by an indirect linear relationship between θ and backscatter σ^0 [42], yielding the so-called *direct slope* β_d (see Figure 4a). However, as a result from the Sentinel-1 acquisition strategy, a reliable slope estimation as linear fit is not possible everywhere for this sensor – in poorly covered areas lacking either sufficient samples or a large enough spread of LIA.

To overcome this problem, a new approach is developed to enable the slope estimation in poorly covered areas. The correlation of slope β with (non-normalised) sensitivity S and mean backscatter $\bar{\sigma^0}$ is for C-band radar found to be in general very high [76]. Thus, at an individual pixel, a linear combination of sensitivity S and mean backscatter $\bar{\sigma^0}$ (i.e. the dynamic range and the all-time mean of the pixel's σ^0-time series) can act as surrogate for the slope, called *regression slope* β_r:

$$\beta_r = a\,S + b\,\bar{\sigma^0} + c \quad [\mathrm{dB}/^\circ] \tag{5}$$

This approach exploits the fact that the predictors S and $\bar{\sigma^0}$ are practically not disturbed by the inhomogeneous coverage of Sentinel-1 and thus can be calculated throughout the area. For clarity, we note that β_d is available only where the coverage is adequate, whereas β_r can be estimated where estimates for S and $\bar{\sigma^0}$ are robust (which is commonly a much larger area).

The coefficients a, b, and c in Eq. 5 are determined in areas with adequate coverage, where it is possible to infer directly the slope β_d from the linear relationship between θ and σ^0. Initially, a multiple linear regression model was formulated, predicting the slope β_d through the available statistical parameters of Sentinel-1 backscatter time series, like mean, sensitivity, standard deviation and other. By support of Monte Carlo methods testing a multitude of linear combinations between them, the regression model as in Eq. 5 was found as optimal, in terms of simplicity and skill to predict β_d. The inclusion of more parameters, or higher-order terms, did not bring significant improvement.

The regression analysis was performed on a Sentinel-1 backscatter dataset at 500m sampling, covering the period October 2014 to October 2016 and a 1200km $\times$ 1200km area in central Europe (Equi7Grid-tiles E042N012T6, E042N018T6, E048N012T6, E048N018T6). The thereof obtained coefficient for Eq. 5 are:

$$\begin{bmatrix} a \\ b \\ c \end{bmatrix} = \begin{bmatrix} -0.01725 \\ 0.00553 \\ 0.02546 \end{bmatrix} \tag{6}$$

The obtained β_r values are used per grid point for the LIA normalisation of the SAR backscatter observations. The reference angle $\Theta = 40^\circ$ is chosen due to its central location in the range of LIA in Sentinel-1 observations, minimising the overall error from extrapolation. With this, all resampled backscatter-values $\sigma^0(\theta, t)$ in the archive are normalised to the LIA of 40° by (see also Figure 4b):

$$\sigma^0(40, t) = \sigma^0(\theta, t) - \beta_r\,(\theta - 40^\circ) \quad [\mathrm{dB}] \tag{7}$$

2) Dry- and wet- reference parameters: To determine with change detection the relative soil moisture content from the SAR observations, one must know the SAR backscatter at dry- and wet- conditions. Ideally, the local backscatter archive spans over a period long enough (e.g. > 10 years) to cover events when the soil is completely dry or saturated, respectively. Then, the lowest and highest values of the time series represent well the dry- and wet- reference parameters (σ°_{dry} and σ°_{wet}). Due to measurements errors, outliers (e.g. from frozen conditions), signal noise, or failing to cover complete dry- or wet- conditions (over arid climates, or when the observation record is too short), this is often ill-posed.

To mitigate this problem, and to reduce the necessary archive length, the algorithm is enhanced in the following way: A grid point's dry- and wet- reference backscatter coefficients are estimated through the 10%- and 90%-percentiles of the normalised backscatter time series ($\sigma^0_{P_{10}}(40)$ and $\sigma^0_{P_{90}}(40)$), assuming that by this choice, the estimation is not violated by outliers. These values are then interpreted as 10% and 90% SSM, and extrapolated linearly to 0% and 100% SSM, respectively (see also Figure 4c):

$$k = \frac{90\% - 10\%}{\sigma^0_{P_{90}}(40) - \sigma^0_{P_{10}}(40)}$$

$$d = 90\% - k\,\sigma^0_{P_{90}}(40)$$

$$\sigma^0_{dry}(40) = \frac{0\% - d}{k} \quad [\mathrm{dB}] \tag{8}$$

$$\sigma^0_{wet}(40) = \frac{100\% - d}{k} \quad [\mathrm{dB}] \tag{9}$$

E. SSM Product Retrieval

The TU Wien Change Detection model attributes changes in normalised backscatter to changes in soil moisture. This is realised by linearly scaling of the actual backscatter between the backscatter coefficients from dry and wet conditions.

1) SSM Estimation: The retrieval of SSM values is performed by application of the scaling equation (Eq 10). With this, the normalised backscatter-value $\sigma^0(40, t)$ is scaled between the two values representing historical driest ($\sigma^\circ_{dry}(40)$) and wettest ($\sigma^\circ_{wet}(40)$) condition at the grid point in question.

$$SSM(t) = \frac{\Delta\sigma^0(40, t)}{S(40)} = \frac{\sigma^0(40, t) - \sigma^0_{dry}(40)}{\sigma^0_{wet}(40) - \sigma^0_{dry}(40)} \quad [\%] \tag{10}$$

Since the dry- and wet parameters are statistically determined, extreme events can lead to SSM values out of the range 0% – 100%. Values that are less than $\pm 20\%$ off-limit are set 0% or 100%, respectively, and values exceeding those extended limits are masked as no-data.

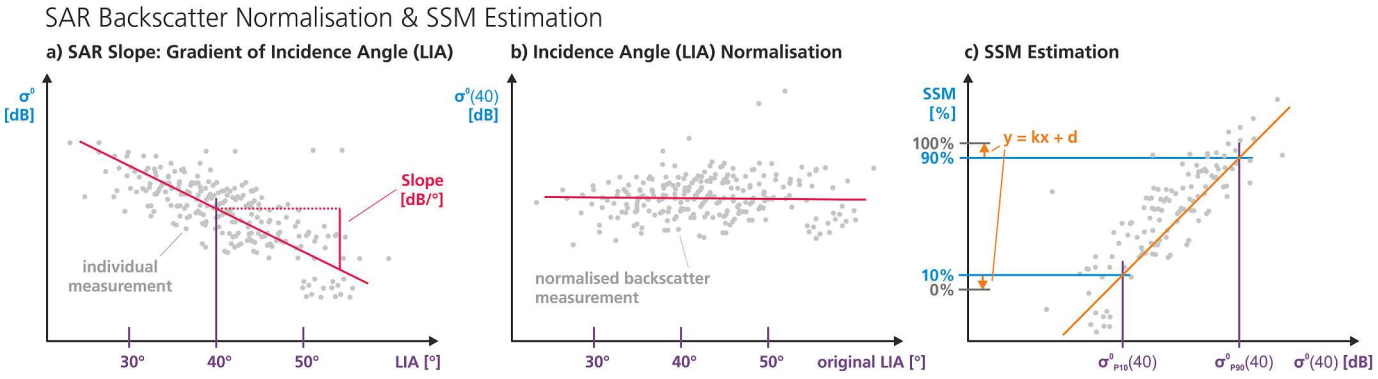

Fig. 4. Sketches for SAR LIA-normalisation and SSM-scaling. (a) The direct slope β_d as linear fit between backscatter and local incidence angle (LIA). (b) Result from conversion of $\sigma^0(\theta,t)$- to $\sigma^0(40,t)$- backscatter through LIA-normalisation as in Eq. 7. (c) SSM from scaling $\sigma^0(40,t)$ between dry- and wet-reference backscatter parameters $\sigma^0_{dry}(40)$ and $\sigma^0_{wet}(40)$, following Eqs. 8, 9, 10.

2) SSM Error Estimation: The SSM retrieval error is estimated through error propagation of the noise of the Sentinel-1 CSAR instrument in IW mode and the respective uncertainties of the model parameters. Following the approach for Envisat ASAR SSM proposed in [42], the SSM retrieval error constitutes of 1) SAR backscatter measurement error $\Delta\sigma^\circ$, 2) dry reference error $\Delta\sigma^\circ_{dry}$, 3) wet reference error $\Delta\sigma^\circ_{wet}$, and 4) slope error $\Delta\beta$, and the errors are assumed to be independent of each other.

Eq. 11 shows the error model from [42], with $\Delta\sigma^\circ$ as the error of the S-1 IW data at 1km, $\Delta\beta$ as the noise of the slope parameter, $\Delta\sigma^\circ_{dry}$ as the error of the dry reference and $\Delta\sigma^\circ_{wet}$ as the error of the wet reference.

$$\Delta SSM^2 = \left(\frac{\Delta\sigma^\circ}{S}\right)^2 + \left(\frac{(\theta-40)\Delta\beta}{S}\right)^2 + \dots + \left(\frac{(SSM-1)\Delta\sigma^\circ_{dry}}{S}\right)^2 + \left(\frac{SSM\,\Delta\sigma^\circ_{wet}}{S}\right)^2 \quad (11)$$

The CSAR sensor's uncertainty in IW-mode is given by the radiometric accuracy with a standard deviation of 0.33 dB for a 10x10m pixel [3]. The noise level of CSAR in IW mode at 1km was already estimated in [48] to be between 0.05 and 0.07 dB. We revised this estimate to $\Delta\sigma^\circ = 0.2$dB after inspection of the data and assuming higher correlations between the errors at the 10m scale.

The uncertainties of the model parameters $\Delta\sigma^\circ_{dry}, \Delta\sigma^\circ_{wet}, \Delta\beta$ are estimated based on assumptions about the potential error sources. Errors can occur in the model parameters due to incomplete sampling over the seasons, which was a problem for Envisat ASAR but is not so problematic for Sentinel-1 CSAR due to the higher and more regular revisit rate. They can also occur due to inherent uncertainties in the statistical methods used to estimate the model parameters. Another error source is the non-dynamic vegetation correction, which leads to seasonally varying errors in the model parameters, which are assumed to more severe for CSAR than for ASAR since observing in VV-polarisation.

Following the reasoning in [42] and [48], we chose the error of the slope to be 10% of the slope parameter, meaning $\Delta\beta = 0.1\,\beta$. The errors for the dry- and wet- references are expected to be 10% of the sensitivity, meaning $\Delta\sigma^\circ_{dry} = \Delta\sigma^\circ_{wet} = 0.1\,S$. The maximum retrieval error occurs either in very dry ($SSM = 0\%$) or very wet ($SSM = 100\%$) conditions and when the incidence angle of an observation is furthest away from the reference angle, at 29.1°. Inserting the assumptions into the error model of Eq. 11 allows an estimate of the maximum SSM error:

$$\Delta SSM_{max} \approx \sqrt{\left(\frac{0.2}{S}\right)^2 + \left(\frac{1.09\,\beta}{S}\right)^2 + 0.01} \quad [\%] \quad (12)$$

F. Static Mask Generation

The Sentinel-1 SSM algorithm does not apply everywhere, or rather does not result in reliable SSM values for every surface, as e.g. water, cities or complex terrain. In example, it is straightforward to mask out water surfaces to remove misleading values over the sea, lakes and rivers.

1) Water Mask: This is facilitated with the SAR backscatter parameters. The water mask is created from the 5%-percentile parameter $\sigma^0_{P_5}(40)$, where each pixel with a value lower than -17dB is classified as water. In the SSM images, those pixels are set automatically to no-data, since SSM cannot be retrieved over water.

2) Sensitivity Mask: The normalised sensitivity $S(40)$ is an important measure for the accuracy and reliability of the Sentinel-1 SSM algorithm. Therefore, a sensitivity mask is generated, masking out pixels with a low sensitivity of CSAR to soil moisture changes. A threshold of 1.2dB is used. This yields a mask that mainly covers urban areas. This mask is stored as auxiliary layer.

3) Terrain Mask: The terrain correction in the pre-processing step does not completely remove errors stemming from topographic effects, owing to azimuthal effects and the insufficient accuracy of available global DEMs. To identify and mask out locations with high topographic complexity, an analysis of the VFP-SRTM90 DEM is carried out and the elevation slope (the gradient) is computed. From this elevation slope, a terrain mask is produced, indicating pixels with an elevation slope higher than 30% (equivalent to a gradient of 17°). This mask is stored as auxiliary layer.

IV. Datasets and Evaluation Area

For evaluating the Sentinel-1 SSM retrieval method, we generated a 3yr dataset over Italy, using all available Sentinel-1A/B observations from Oct 2014 – Oct 2017. A comprehensive evaluation of remotely sensed SSM data requires a reference dataset of comparable spatio-temporally density and coverage. Here, we used the Soil Water Balance Model (SWBM, [77]) and carried out an in-depth analysis of the signal quality over the Umbria region in central Italy, validating the S-1 SSM data against the model data, as well as against reference from in-situ and satellite observations.

A. The 1km Sentinel-1 SSM Dataset: S-1 SSM

For the evaluation, all available Sentinel-1 IWGRDH observations over Italy, which were quality-checked and eligible for the SSM retrieval, were processed with the algorithm in Section III. The obtained data cube comprise SAR imagery over five Equi7Grid-tiles (each 600km wide), with 180 to 420 single observations per 500m pixel (average 291) from the period Oct 2014 – Oct 2017. From the pre-processed SAR backscatter data cube, we generated the SSM parameters as described in section III-D, yielding a set of four parameters and three masks per Equi7Grid-tile. Finally, we retrieved the SSM images for each input SAR image. We masked the SSM data for complex terrain, water and low sensitivity as described in section III-F.

Figure 5 displays the S-1 SSM model parameters generated by the algorithm in section III-D over Italy and its neighbours, along with the Sentinel-1 coverage and land cover from CORINE [74] for comparisons.

The number of available Sentinel-1 scenes (Figure 5a) is a function of the Sentinel-1 observation pattern, ranging from 180 to 420 measurements in 3 years. Also, it is obvious that the inclusion of Sentinel-1B observations is perpetuating the inhomogeneous coverage of the satellite mission. The Umbria region showcases the challenges coming from the inhomogeneity, as comprising in small space the full range of observations number. The Terrain Mask, generated by methods described in section III-F, marks many pixels along the Alps and the Apennines, as well as great portions of Corsica. The Sensitivity Mask basically marks pixels in and around cities and coastlines. Both masks work as desired, to exclude pixels from the product where the S-1 SSM retrieval is insensitive to soil moisture changes.

Figures 5b-c show the inputs for the dry- and wet references that hold the average backscatter values under dry- and wet conditions, respectively. They comprehend many patterns reflecting geographic features that are governed by topography and land cover, but seem to be free of artefacts stemming from the inhomogeneous coverage pattern. Apparently, the 3yr S-1 backscatter archive allows already a robust estimation of the parameters. When compared to the land cover (as in Figure 5f), the dry-reference values are in general higher over cities, and lower in agricultural areas (for example the Po Valley in central-northern Italy, or the area east of Vienna in the north-eastern corner of the image). Along the Alps, and also along the high ranges of the Apennines, the dry-reference is also very low, likely due to the prevalence of wet snow conditions. The wet-reference shows high values over cities, too, but lower values over forests (e.g. at the margin along the Alps), and moderate values over agricultural areas.

The SSM sensitivity (Figure 5e) is the difference between the dry- and wet-reference and reflects the algorithm's ability to sense SSM changes, constituting a quality indicator. Fortunately, the sensitivity is clearly high over flatlands and agricultural areas, which of special interest of many users, but also over the central Alps. The latter results from the large range between wet and dry (or no) snow that commonly governs the backscatter of the Alps' higher altitudes. Hence, the Terrain Mask is of particular importance over high mountain ranges. In Umbria, only parts of the region feature high SSM sensitivity, whereas the in-situ station in Emilia-Romagna is located in the Po Valley, an area featuring almost entirely high sensitivity.

The SAR Slope (Figure 5d) is the parameter used for normalising the backscatter data for the radar local incidence angle (LIA), with the latter being a function of the satellite orbit geometry and the terrain. The here generated regression slope (following section III-D1) shows a higher dependency of S-1 SAR measurements on the LIA over cultivated areas and the central Alps. The reason for the first is to a great portion the presence of crops and other low vegetation, acting often as non-lambertian microwave scatterers. The reason for the strong slope over higher ranges of the Alps is the incapacity of the regression approach to model the slope where a snow cover is prevalent. This becomes evident when comparing the S-1 slope with historic slope estimates from Envisat ASAR WS (Wide Swath mode) from the years 2005 – 2012 (see mini map at Fig. 5d). This reference dataset on the one hand confirms most of the spatial patterns in the S-1 slope obtained by regression approach, but on the other hand shows a completely different slope over the Alps (albeit noisy and erroneous, too). In conjunction with the issue that radar remote sensing over strong topography is in general error-prone [38], this encourages us in applying the Terrain Mask consequently.

Moving now on to the resulting S-1 SSM data, Figure 6a shows an monthly mean SSM image of Italy and its neighbours for July 2017, when the area was struck by a persistent drought. The monthly mean image allows full coverage of the area (in contrast to single observations) and reflect well the extraordinary dry conditions in Italy at that period, especially in the east-central regions of Tuscany, Umbria, and Lazio. The minimap in Fig.6a provides as reference the 2017 July mean SSM from ASCAT (see Section IV-E), widely confirming the general SSM pattern in the Sentinel-1 data. While the known issue of wet biases around larger cities is present in the ASCAT data (e.g. around Munich or Vienna in the north), it suggests even drier soils over Italy in that period. Since the SSM-levels agree well in the other areas, the longer parameter baseline of the ASCAT sensor (which observes since 2007) presumably covers more extreme conditions and hence allows the ASCAT product to estimate more accurately the drought's severity.

Figure 6b zooms into the Po Valley on July 10-11th, where a rainfall event, as recorded by interpolated terrestrial rainfall observations of the Department of Civil Protection in Italy, is well captured by two consecutive S-1 SSM images. The

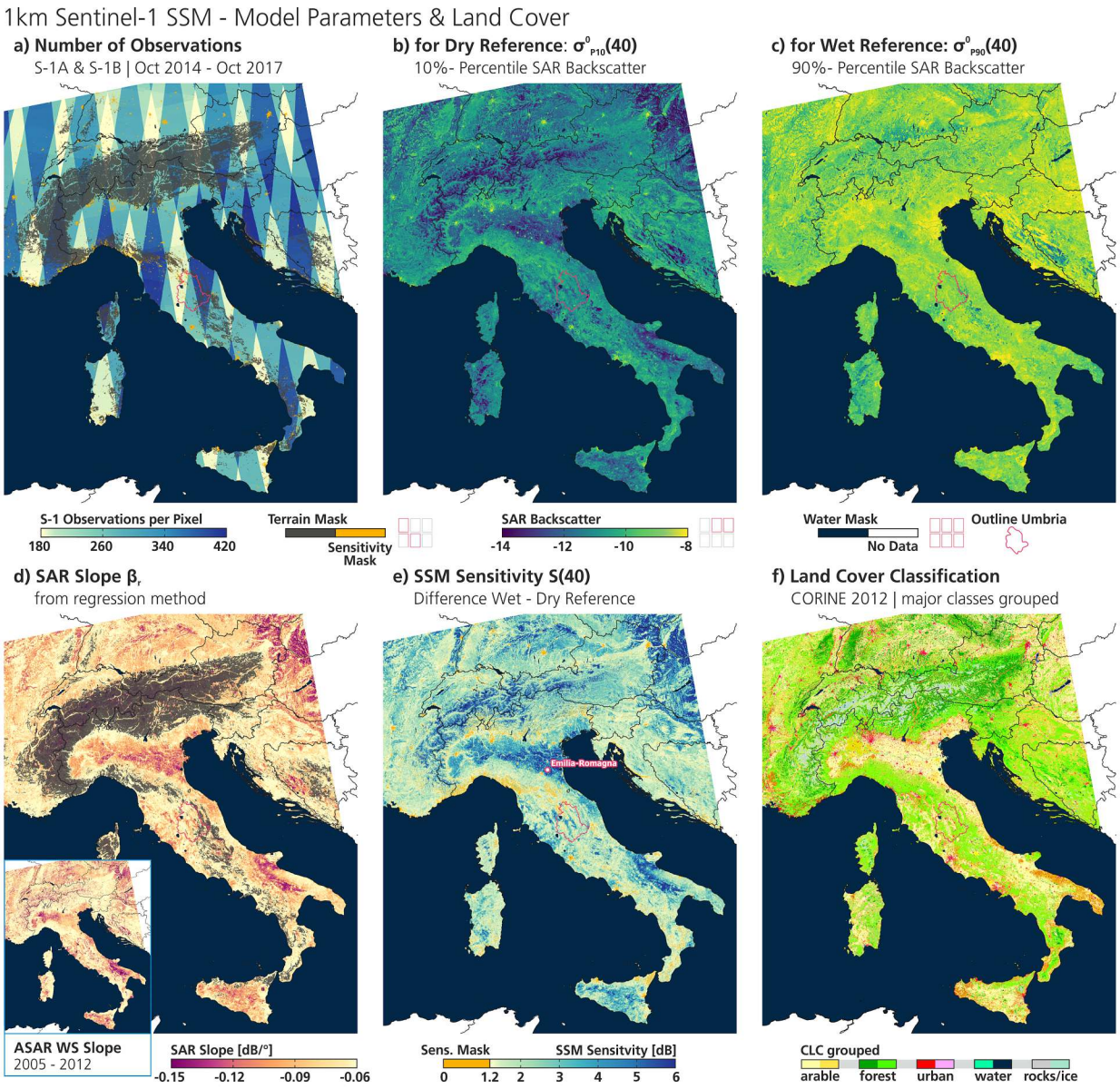

Fig. 5. Collection of S-1 SSM model parameters, and for comparison land cover, at 500m-sampling. (a) Number of observations from Sentinel-1A and -1B during the evaluation period, overlaid with Terrain Mask and Sensitivity Mask. (b) for the dry-reference, the 10%-percentile of normalised SAR backscatter. (c) for the wet-reference, the 90%-percentile. (d) the Regression SAR Slope, with historic slope estimates from Envisat ASAR WS (Wide Swath mode) in the lower left. (e) SSM Sensitivity, overlaid with Sensitivity Mask and location of Emilia-Romagna in-situ-station. (f) CORINE 2012 land cover classes as major groups.

24h-cumulative precipitation image marks out rainfall areas, whose outlines correspond well with areas in the SSM data that changed from dry to wet soil. Analysis at this resolution of rainfall-induced soil moisture changes is not possible with established remote sensing SM products, e.g. from Metop ASCAT or SMOS (not shown).

Figures 6 h) and i) show example S-1 SSM images retrieved from data sensed by Sentinel-1B the ascending overpasses on 2017-05-07 and 2017-06-05 at ca. 17h. The extents of the SSM images illustrate the coverage of Sentinel-1 from single overpasses. The first image from May shows contrasted large-scale SSM patterns north of the Alps in Bavaria and Upper Austria, while over central Italy contoured paths of rain showers, which crossed the area on that afternoon (as reported from meteo-data, not shown), are evident in the SSM image. The second SSM image from June shows rather wet conditions north of the Alps in southern Germany, as well as at the southern fringe of the Alps in the Lombardy region. Weather records (not shown) report heavy local rainfall events in the area, reflected by the SSM data as scattered wet-spots in a general dry setting in central-northern Italy. The value of the Terrain Mask becomes evident when focusing on the boxed Alpine section, showing unmasked version of the SSM data. Over strong topography, the radiometric correction of the radar response and the LIA-normalisation are failing and create noisy data. The Water Mask appears to correctly take out pixels over the sea or lakes, reproducing well the coastlines of the Mediterranean or the lakes in the Alps and in central

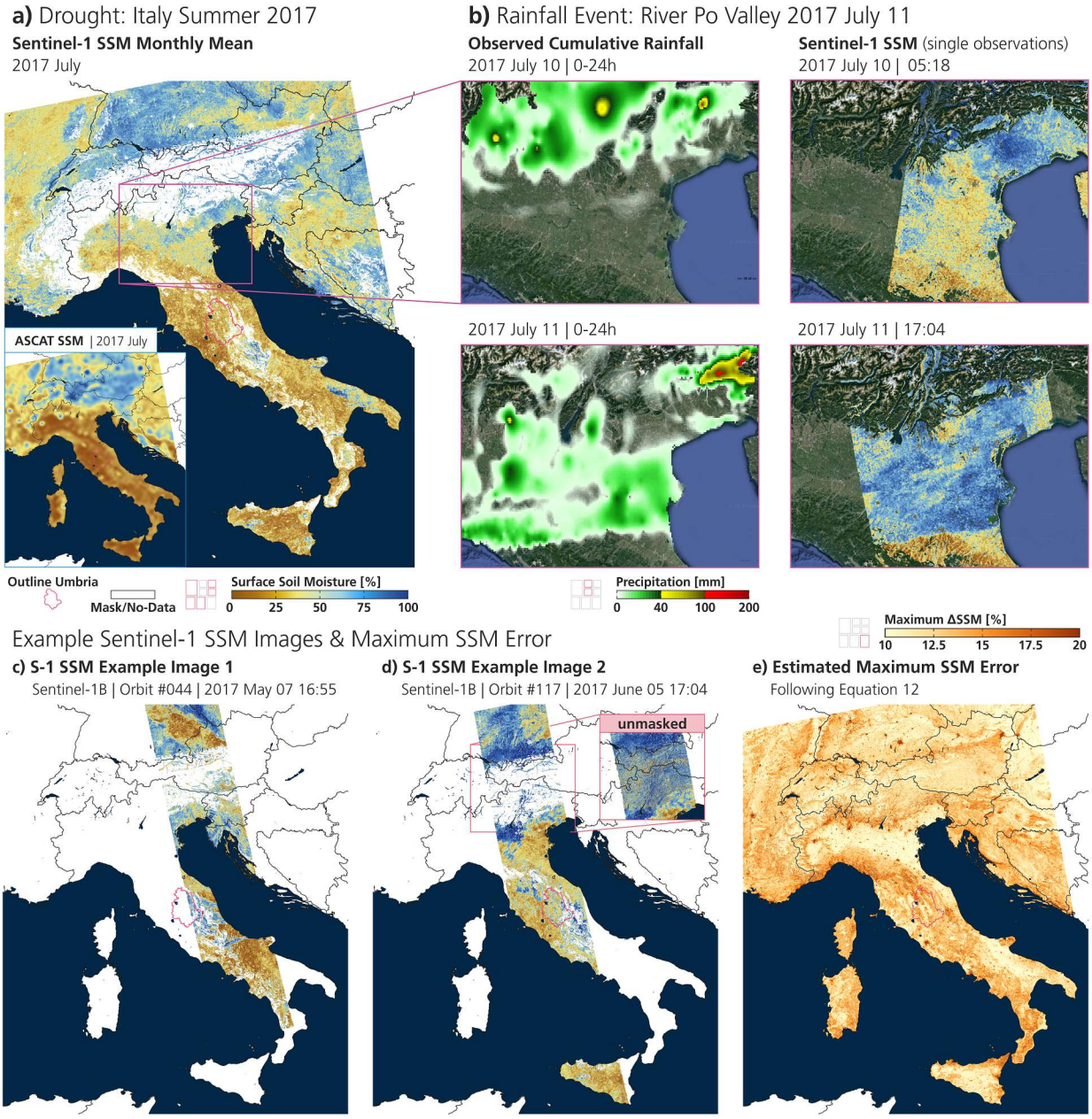

Fig. 6. (a) Monthly mean SSM image over Italy and neighbouring countries for July 2017. Masked areas, and areas outside of the dataset domain, are displayed in white. The region of Umbria is outlined in red. (b) Zoom into the Po-valley on July 10-11th, with cumulative rainfall from terrestrial rainfall radars on the left, and single Sentinel-1 SSM observations on the right. Basemap from Google Earth. (c) Example S-1B SSM masked image from 2017-05-07, afternoon overpass at 17h from orbit Nr.117. (d) As (c) but for 2017-06-05, and with detail over the Alps showing unmasked version. (e) Maximum error in SSM following Eq. 12.

Italy.

Finally, Figure 6e maps the potential error of the SSM product over the study's data domain. These estimated maximum SSM errors are calculated with Eq. 12. The values range from 10% to 20% SSM and reflect the error under the most unfavourable measurement configuration, assuming extreme observation angles and extremely dry or wet soils. One can see that the SSM error is strongly related to the SSM sensitivity, with relatively good conditions over e.g. the Italian valleys, or western Slovakia/Hungary and the surroundings of Vienna in the north-east. Zooming into Umbria, and with regard to the land cover showed in Fig.5f, we see that the estimated error is low over the agriculturally used lowlands and high over the forested hills (see also Figure 8 and the next section).

B. Study Area: Umbria Region

The Umbria region in central Italy has a complex landscape topography and it is characterized by terrigeneous facies and flysch deposits. The soil, overlying practically impervious rocks, is composed of clay and sandy silt. The main land uses are woods (42.6%), and crops (49.2%) that are mainly located in the flat area, whereas urban areas cover only 3.5% of the

territory. Forests are generally located in headwater areas and crops in the low-lying areas. See in Figure 8a the region's topography, and in Figure 8b its land cover as from CORINE 2012 [74].

The climate is Mediterranean, with mean annual rainfall of ca. 950 mm. Precipitation ranges over the study area between 650 mm and 1600 mm (based on the period 1951-1999 and on a network of more than 60 raingauges). Higher monthly rainfall values generally occur during the autumn-winter period. In this period floods normally occur, caused by widespread rainfall. The mean annual air temperature (for the period 1951-1999) ranges between 3.5C° and 14.0C°, with a maximum in July and a minimum in January. Accordingly, the mean annual potential evapotranspiration, computed with the Thornthwaite formula, is, on average, about 800 mm.

A dense real-time hydrometeorological network (1 station every 150km^2) has been operating in the Umbria region for more than 20 years which currently consists of 90 raingauges, 77 thermometers and different 12 soil moisture stations distributed throughout the territory [78]. The monitoring network provides semi-hourly data for which a quality-check step is performed in order to remove anomalous values and to fill any temporal gaps.

C. Model Data: SWBM-SA Umbria

We used modelled 1km soil moisture (Model SM) estimated with semi-analytical SWBM (SWBM-SA, [79]) to test the ability of the S-1 SSM data to reproduce the temporal and the spatial variation of SM. The structure of the SWBM was derived from an extensive study carried out in an experimental catchment located in Umbria, so the model is specifically suited for providing reliable SM estimates in this region [77]. It has been applied also in different test-sites located across Europe, obtaining a good performance in all of them, with correlations higher than 0.8–0.9 and RMSDs lower than 0.025m^3/m^3 [79]–[81].

For this study, interpolated 1km rainfall and temperature data drove the SWBM-SA model, yielding hourly-based SM estimates on a 1 km-based regular grid for an area of 8991km^2 (Figure 8). The mountainous eastern part of the region was intentionally excluded as the density of rain gauges here is much lower and the Sentinel-1 observations are expected to be largely impacted by the topography. Input precipitation and temperature data cover the period 2014-2017. Input soil model parameters were specifically built for Umbria region (outlined in [78]). SM estimates were produced for the topmost 10cm of the soil, to minimize the depth mismatch with S-1 SSM (topmost 5cm).

D. Insitu Data: ISMN

In-situ data from the International Soil Moisture Network (ISMN, [82]) were used for evaluation (In-Situ SM). The ISMN provides a harmonised repository of in-situ soil moisture observations all over the world and is well-evaluated and established in the community [83]–[85]. Here, we use five UMBRIA-stations from the Umbria region and one COSMIC-station, close-by in the Emilia-Romagna region (see Fig. 8a).

During the analysis period, only five out of twelve UMBRIA-stations measured soil moisture, some of them discontinuously, or not during the full period. The five instruments consist of four Frequency Domain Reflectometry (FDR) stations and one Time Domain Reflectometry (TDR) station with sensors located at different depths (5-40 cm). Three stations (Cerbara and Torre dell'Olmo and Petrelle) are operating in real-time and provide measurements every 30 minutes. For the validation of Sentinel-1 SSM data, we used only measurements at a depth of 10cm. The two stations in the east of Umbria are located in a section of good coverage by S-1 (Foligno, Torre Dell'Olmo with 401 measurements), the other three in the north-west were measured only half as often (Cerbara, Monterchi, Petrelle with 198 measurements).

The COsmic-ray Soil Moisture Observing System (COSMOS) is a network of stations that measure soil moisture through a newly-developed cosmic-ray method [86]. The stationary cosmic-ray soil moisture probe measures the neutrons that are generated by cosmic rays within air and soil and other materials, moderated by mainly hydrogen atoms located primarily in soil water, and emitted to the atmosphere where they mix instantaneously at a scale of hundreds of meters and whose density is inversely correlated with soil moisture. This measurement scale makes it a valuable reference for the remotely sensed 1km S-1 SSM.

We used the station Water4Crops Budrio IT (098), located in Emilia-Romagna in the Po Valley in an extremely flat area with intensive, irrigated agriculture. The site is a test site for different irrigation techniques and different water sources (reuse of treated wastewater) and has a mean annual precipitation of about 750 mm with a mean annual temperature of 16.0C°. The station provides measurements of soil moisture in the range of 0–21cm and data are available from about 2014 to 2016. This station is located in section of medium S-1 coverage (286 measurements).

E. Satellite Reference: ASCAT SSM

As reference satellite data, we uses SSM data derived from the Advanced SCATterometer (ASCAT) on-board the Metop polar-orbiting satellite series (Metop-A/B/C). The ASCAT sensor is an active microwave remote sensing instrument operating at C-band (5.255 GHz) in VV polarization. Thus, this sensor is very similar to the Sentinel-1 CSAR, but with a substantial lower spatial resolution and higher temporal revisit time. It has proven to be a valuable instrument monitoring soil moisture changes over the land [81], [83], [87], employing the TU Wien backscatter model, too.

The Metop ASCAT SSM dataset was provided by the EUMETSAT Satellite Application Facility on Support to Operational Hydrology and Water Management (H-SAF) service[7]. The H111 product was selected, a global Climate Data Record (CDR) of Metop ASCAT 25km SSM time series at 12.5 km sampling on a discrete global grid (DGG), covering the period 2007 – 2016. The H-SAF SSM CDR is released each year end of January providing most complete and consistent SSM information. The product contains SSM retrieved from

[7]http://hsaf.meteoam.it/

all orbiting Metop satellites if the calibration between the instruments has proven to be consistent.

V. Evaluation

We evaluated the S-1 SSM data against soil moisture data from the model-, satellite-, and in-situ-datasets presented in above Section IV. Also, the new Dynamic Gaussian Upscaling (DGU) method for downsampling Sentinel-1 images was evaluated.

A. Preparations

The different soil moisture products are characterized by different measurement units and have different grids. Thus, we reprocessed them for a meaningful comparison.

a) Data Matching to Reference: In particular, the comparison of S-1 SSM and ASCAT SSM data with the reference data required the following steps: 1) Spatial matching: The satellite pixel of ASCAT and S-1 whose centroid is nearest to the reference location has been selected and the corresponding relative SSM time series has been extracted. 2) Temporal matching: The site-specific soil moisture data closer to the corresponding acquisition time of S-1 and ASCAT were extracted from their time series. Flagged data due to water, sensitivity or complex terrain, or out-of-bound values, were masked out. 3) Conversion to volumetric SM units: Following [88], per pixel, the mean and the variance of S-1 SSM and ASCAT SSM (both in relative units) were matched to those of co-locating reference data to transfer the values to the absolute domain with the unit m^3m^{-3}. The model-data-grid-points are already co-locating with the Sentinel-1 pixels, thus spatial matching (step 1) was not necessary for the evaluation against the model.

b) S-1 SSM Upscaling to 25km: For an additional comparison to ASCAT SSM, a spatial upscaling of S-1 SSM from 1km to 25km was done, following the Gaussian method described in Section III-C (without pixel masking). With this, we minimise effects from the different measurement scales and can assume the same representativeness errors.

For evaluating the SAR backscatter upscaling from 10m to 500m sampling, we analysed 29 Sentinel-1 IWGRDH images, distributed over the period Feb 2016 – Nov 2016 and major European regions. Two independent upscaling runs were applied to the images, yielding two sets of 29 images at 500m sampling: 1) Run in sequence *filtering–aggregation*: First filtering the 10m pixels with an 171×171 Gauss-kernel and than aggregating them to 500m pixels (as suggested by theory). 2) Run in sequence *aggregation–filtering*: First aggregating them and then filtering with the 3×3 Gauss-kernel from Equation 4 (as applied in the S-1 SSM algorithm). The dynamic masking of extreme values at the 10m sampling was done identically in both runs.

B. SAR Upscaling Performance

According to theory on image sampling, the filtering must be applied before the aggregation when downsampling/upscaling an image [56]. Regardless of this, the Dynamic Gaussian Upscaling (DGU, section III-C) first aggregates the pixels and then applies the (coarse) filter in order to speed up the processing. We tested the DGU method for a set of 29 Sentinel-1 IWGRDH images.

The comparison of the two upscaling procedures at hand, the sequence *aggregation–filtering* against the sequence *filtering–aggregation*, shows the following:

1) The processing time, excluding reading/writing operations, is reduced by factor 9.
2) The median RMSD between the two output sets is 0.05dB.

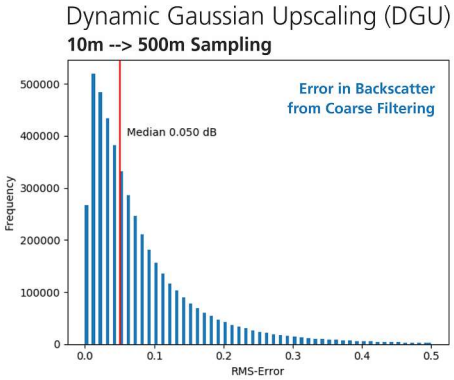

Fig. 7. SAR resampling from 10m to 500m: Root Mean Square Difference (RMSD) in backscatter between output from the sequence *filtering–aggregation* and the sequence *aggregation–filtering* (coarse, fast filtering).

Figure 7 shows the distribution of the RMSD between the two sets of backscatter images. Overall, the errors are of the same magnitude as the sensor's noise level at the 1km scale (0.05dB to 0.07dB estimated by [48], revised to 0.2dB by us), with most of them smaller, and thus can be regarded as insignificant. The savings in computation time, however, are substantial and constitute a major algorithmic improvement.

C. S-1 SSM Signal Quality: Umbria Model Domain

Main results from the evaluation of the S-1 SSM data against the Umbria Model SM are displayed in Figure 8, with statistics summarised jointly with the analyses at the in-situ stations (Section V-D) in Figure 9, comprising the Pearson-R distributions as well as mean RMSD values in m^3/m^3.

Fig.8c is a plot of the Pearson correlation coefficients (R) between the satellite and the model data, mapping 8991 1km grid pixels. The median R-value is 0.38 (mean RMSD=$0.099m^3/m^3$), suggesting only medium agreement between the two datasets. However, a clear pattern of higher R-values is detected, reproducing geographic features in the topography map in Fig. 8a and in the land cover data in Fig. 8b. It appears that the S-1 SSM shows higher agreement with the model in the lowlands that are used agriculturally. In particular the areas classified by CORINE as arable stand out in the correlation map in Fig.8c, whereas forested areas show low R-values, confirming the insights from analysing the SSM sensitivity and SSM maximum error in Fig.5.

The land-cover-driven behaviour of the S-1 SSM is as expected, as there are similar results documented for previous

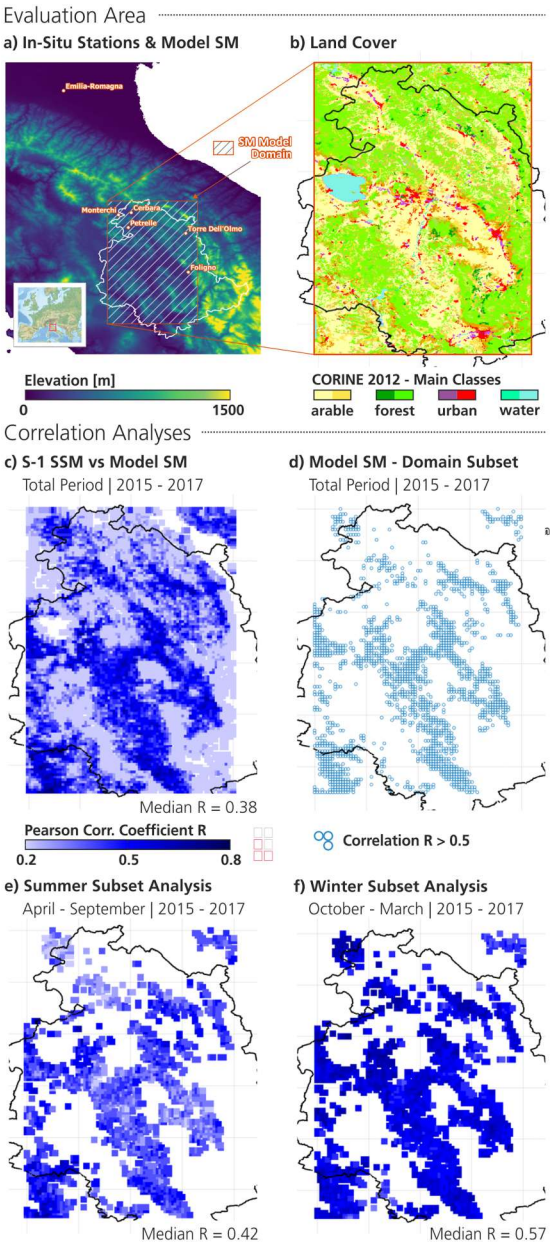

Fig. 8. (a) Evaluation area over Umbria, with Model SM domain, in-situ stations, and COSMOS-station in Emilia Romagna. Elevation map as background. (b) CORINE Land Cover, grouped to main classes occurring in the area. (c-f) Results from the comparison of S-1 SSM with Model SM, showing the Pearson R over the full model domain (c), the subset of grid points with high R (d), the summer analysis (e) and the winter analysis (f) of the subset grid points.

C-band missions as e.g. Envisat ASAR. The radar interactions with forests are not straightforward and the S-1 SSM sensitivity is as expected low. Certainly, the performance is higher over areas with less vegetation density, demonstrated by the map in Fig.8d, showing all grid points with a R-value higher than 0.50, clearly resembling CORINE's arable classes. This underlines that the current S-1 SSM product is not capable of estimating SSM over dense vegetation like forests. For further analyses against the Umbria model, we narrowed down the spatial extent to this subset domain, focusing on the performance over agricultural land.

That followed, we expect also a seasonal component in the signal quality, as vegetation dynamics are not modelled by the algorithm yet. Indeed, the season-separating analysis in Fig.8e-f show lower R-values during the summer months (April to September) than during the winter months (October to March) over the subset area. As this is mainly agriculturally used land, this indicates that the vegetation variation interferes with the S-1 SSM signal during the growing season. The hypothesis that such effects are weaker during the winter months is supported by the higher agreement for this period (median R=0.57, mean RMSD=0.076m^3/m^3).

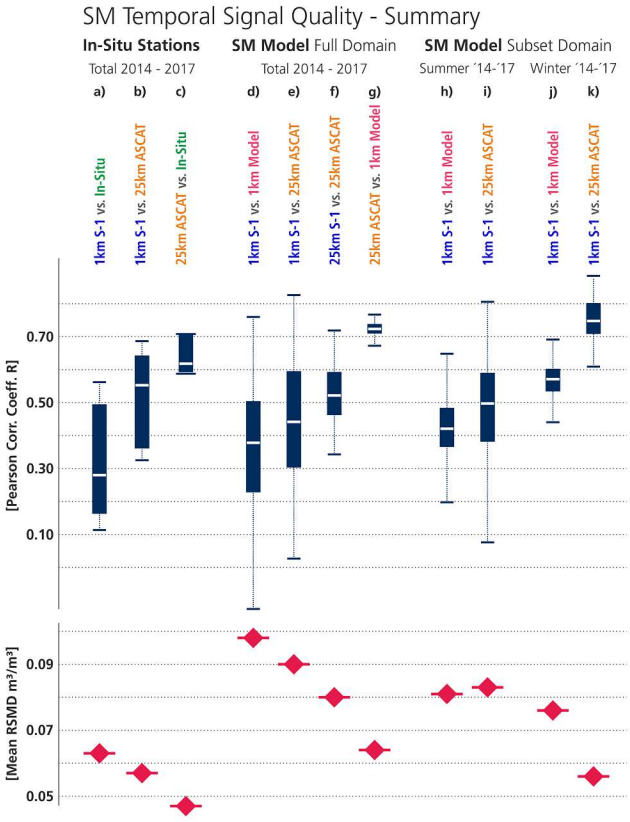

Fig. 9. Compilation of statistics on Pearson R-values and average RMSD from the temporal analyses between S-1 SSM and references (Model SM, ASCAT SSM, In-Situ SM) over in-situ stations (a-c) and the Umbria SM model (d-k).

Analogue analyses over the Umbria model between S-1 SSM and ASCAT SSM endorse above findings, albeit with higher R-values (full model domain, median R in total period: 0.45 (mean RMSD=0.090m^3/m^3), in summer: 0.49 (mean RMSD=0.083m^3/m^3), in winter: 0.75 (mean RMSD=0.056m^3/m^3); maps not shown; statistics see in Figure 9e, i, k). The S-1- and ASCAT- SSM-retrievals are very akin, but one major difference is the absence of a dynamical vegetation correction in the Sentinel-1 algorithm. Thus, this comparison against ASCAT SSM further indicates an interference of vegetation dynamics with the SSM signal as captured by S-1 during the growing season. Obviously, as being based on the same measurement principle and similar SSM modelling, the overall agreement is higher with ASCAT than with the model data (median R=0.45 vs. 0.38; mean

RMSD=0.090m^3/m^3 vs. 0.099m^3/m^3). To suppress the scale mismatch, an upscaling the S-1 SSM data to the 25km-scale of the ASCAT observations was done, yielding a median R of 0.52 and a mean of RMSD=0.080m^3/m^3 between 25km S-1 SSM and ASCAT SSM (Figure 9f). We classify this as a good result, considering the large share of forest and crop areas in the model domain. We assess from this result also that implementing a vegetation correction in the S-1 SSM algorithm would potentially improve the overall signal quality over vegetated areas.

ASCAT SSM itself shows high agreement with the Model SM, with an median R of 0.72 (mean RMSD=0.065m^3/m^3; Figure 9g), giving us confidence in the signal quality of the two reference datasets over Umbria.

D. S-1 SSM Signal Quality: In-Situ Stations

Figure 9a-c and Figure 10 display representative results from the evaluation of the S-1 SSM against the reference data at the in-situ stations. Overall, the agreement between S-1 SSM and In-Situ-SM is low (median R=0.29, mean RMSD=0.088m^3/m^3), contrary to the comparison with ASCAT SSM at these locations (median R=0.56, mean RMSD=0.070m^3/m^3). The ASCAT SSM product itself seems to agree well with the ground data (median R=0.63, mean RMSD=0.056m^3/m^3), but less than with the Umbria model, though.

Comparisons of remotely sensed SM data to point-like ground data is often somewhat troublesome due to the scale mismatch, but the (larger-scaled) signal from the COSMOS-station in Emilia-Romagna from Jul 2015 – Aug 2016 is relatively well reproduced by the S-1 SSM data (R=0.49, RMSD=0.032m^3/m^3) Figure 10a). Also the ASCAT SSM signal, which was available for a longer period, is comparatively well reproduced (R=0.62, RMSD=0.027m^3/m^3). Even individual peaks are captured, commonly stemming from rainfall events. At this location, which is defined by flat terrain and intensive agriculture with irrigation practices, the S-1 SSM shows a similar agreement with the ground data as the well-proven ASCAT product (R=0.58, RMSD=0.028m^3/m^3).

The Torre Dell'Olmo station was recording SM during the entire validation period (Figure 10b). Here, the S-1 SSM seems to miss the SM signal (R=0.11, RMSD=0.085m^3/m^3). However, inter-comparison of the two satellite products yields much higher correlation (R=0.64, RMSD=0.056m^3/m^3), letting us speculate that a scale mismatch troubles the comparison, as also the ASCAT shows relatively low agreement (R=0.60, RMSD=0.059m^3/m^3) with the in-situ point data. From the time series plots, also a distinct positive bias during summer 2015 is evident in the S-1 SSM data. As this is not the case for 2016 or 2017, more knowledge on the local cultivation and crop rotation could give insight on this potential vegetation bias. However, from 2016 ongoing, the temporal dynamics of the S-1 SSM appear overall to follow a more distinct pattern, with less noise-like variation. The inclusion of Sentinel-1B data, starting in Oct 2016, enhances significantly the density of observations.

Similar observations can be done at Foligno station in eastern Umbria (Figure 10c), where we found a similar positive

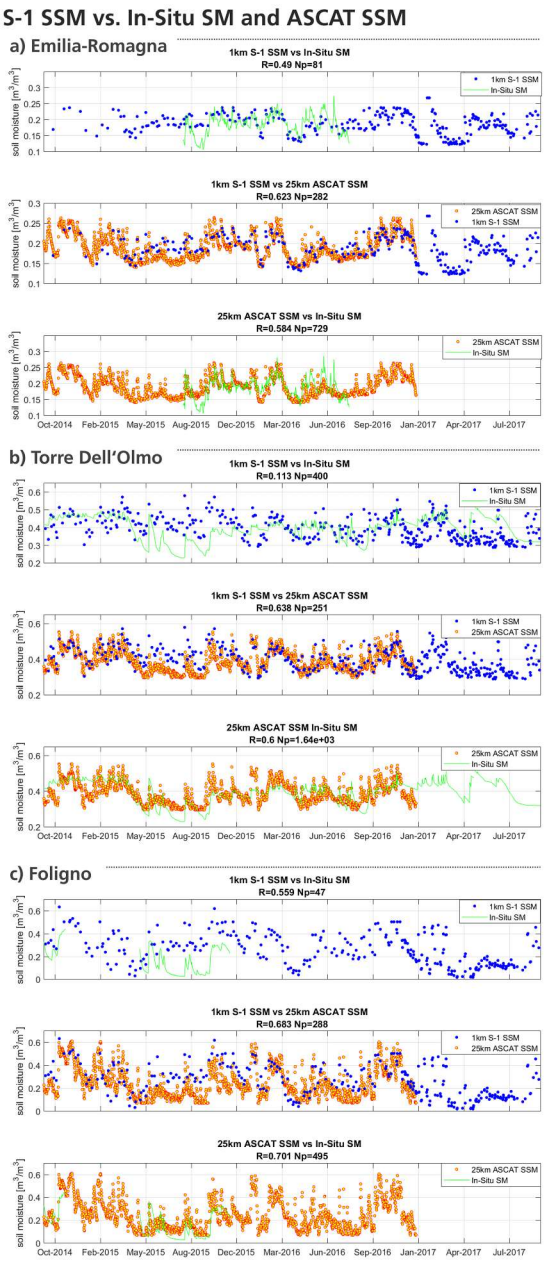

Fig. 10. Comparisons of time series of S-1 SSM with references (In-Situ SM and ASCAT SSM) at selected in-situ stations. Values in volumetric units [m^3m^{-3}]. All available data for the period 2014 – 17 are displayed. With Pearson corr. coeff. (R) and associated sample number of temporally matched data (Np).

bias in the S-1 SSM data for summer 2015, which is not case for the ASCAT SSM. While the evaluation against the short in-situ data is not very meaningful, the agreement with ASCAT is again high (R=0.68), but with a substantial (mostly positive) bias (RMSD=0.133m^3/m^3). The distinct drop of SM levels in March 2016, as observed at all stations, and by all reference data, is again well reproduced by the S-1 SSM.

Above findings are widely supported by the time series analyses at the remaining three stations, which are included in the statistics in Figure 9 (time series plots are not shown).

VI. Conclusions and Outlook

In this paper, we report on the Sentinel-1 mission and its suitability for global soil moisture monitoring, continuing the legacy of ERS-1/2 and Envisat ASAR into the next decade. We discuss how the mission's satellite- and sensor- configuration lays the foundation for operational global monitoring, how the high-resolution CSAR backscatter measurements can be used to retrieve soil moisture at the kilometric scale, and how the processing can be carried out in an efficient manner. The presented S-1 SSM retrieval algorithm, based on the well-established TU-Wien backscatter model, consolidates the knowledge gained during the examination of the Sentinel-1 mission characteristics and data record, and migrates successfully the retrieval method to the new sensor.

Several steps had to be taken in order to formulate the current algorithm.

1) The high spatial resolution of the Sentinel-1 CSAR imagery brings the benefit of very detailed information on the soil properties, but comes at the cost of high signal complexity and large data volume. Here, the Dynamic Gaussian Upscaling (DGU) method, with the dynamic masking of non-soil pixels and the efficient downsampling, enables a most correct and fast upscaling of the 10m sampled input images to a 500m sampling (featuring a 1km resolution), while exploiting the high level of detail provided by S-1. The evaluation of the DGU method showed very satisfying results, as the computation cost could be reduced significantly (factor 9), while the errors in backscatter are negligible.

2) The speeded up computation is especially important in the light of the encountered large data volumes produced by the S-1 CSAR sensors, when the aim is a daily processing of continental or global coverage in near-real-time (NRT). When employing one computer node, the DGU downsamples one S-1 IWGRDH image in ca. 1min (instead of ca. 10min) and hence reduces time pressure on the NRT-processing-facility. Apart from that, the S-1 SSM algorithm with its design suitable to a tiled data-cube architecture, here realised by the Equi7Grid, supports parallel processing and lays the foundation for successful NRT operations employing HPC systems.

3) The repeating orbit geometry of S-1 constitutes a major challenge when estimating SSM through SAR change detection: First, the normalisation of the SAR measurements for the local incidence angle (LIA) is not possible with methods used for precursor sensors. A new approach to obtain the SAR slope through regression from stable SAR parameters was proven successful. The so-called regression slope enables the LIA-normalisation of Sentinel-1 observation not only in well-covered sections, but also in the poorly covered sections. However, backscatter over strong topography is still wrongly normalised, but on top of an enhanced model for snow areas, one would require azimuthal modularisation to be taken into account, too. A current study [89] tackles this problem, as it examines the orientation of the slope and discusses a new method to simultaneously normalise for the incidence- and the azimuthal- angle of a Sentinel-1 measurement.

4) The second impact of the repeating S-1 orbit geometry is the inhomogeneous coverage pattern, which will persist in time. However, a general insight from the examination of the obtained parameters is that the inhomogeneity of the S-1 coverage does not lead to a defective parameter set, suffering from e.g. strip-wise discontinuities. With three years of data over Italy (which is i.g. less often overpassed than northern areas), the S-1 SSM algorithm estimates reliably and consistently slope and reference parameters, effectively coping with the unequal coverage. Hence, only the varying observation frequency remains in the SSM data, leading to a varying temporal resolution around the area, equivalent to a range of frequency from 1.5 to 4 days over Europe.

5) The dry- and wet-references of the SSM model are now determined by the 10%- and 90%- percentile of the local backscatter record, enabling a more robust estimation of these parameters. However, an absence of pronounced dry- and wet conditions in the data record period could still incapacitate the algorithm. With the relatively short S-1 data archive, the severity of extreme events may be under- or overestimated, but the percentile-approach seem to be helpful in reducing the necessary archive length.

6) The production of masks for troubling terrain, low sensitivity and water bodies was introduced and found to be valuable to the SSM product during the evaluation. Here, we identify the masking of frozen soil and snow cover as further important addition to the algorithm, as radar measurements of frozen surfaces can impair significantly both the SSM estimates and the model parameters. Work on masking for frozen soil through detection of snow and freeze/thawing conditions was already done for Metop ASCAT [90], and is envisaged now for migration to S-1. Also, an integration of external remote sensing data on snow cover and soil temperature bears much potential, as such data is more and more available on the kilometric scale.

The evaluation of the S-1 SSM's signal quality over Italy yielded satisfying results, considering the challenging topography and land cover over Umbria. While the agreement with the ground data at the Umbria in-situ stations is on average low, the product shows moderate to high agreement with the 1km model data, especially over non-forest areas. We foreground the comparison with the model data, as the spatial representativeness of modelled soil moisture values matches the S-1 SSM's resolution. This is supported by the results at the COSMOS-station, where the sensor is also measuring soil moisture over a greater area, representing some hundreds of meters. Here, the agreement of the Sentinel-1 product with the ground data is at the same level (similar correlation; with smaller bias) as it was found for Envisat ASAR SSM over Oklahoma [42], a more favourable area for remote sensing of soil moisture, as featuring no strong topography and less share in forest area. The comparison with ASAR SSM is specifically interesting, since it ingests HH-polarised SAR data that is much less sensitive to vegetation influences. Indeed, the S-1 product, based on VV-polarised data, does not reliably detect SSM changes in densely vegetated conditions. Furthermore, over agricultural areas, it wrongly attributes vegetation dynamics, in form of changes in plant stature and water content, to SSM dynamics, potentially inducing a positive bias during

the growing season.

On these grounds, enhancing the algorithm with a dynamic vegetation correction would constitute a major quality boost. This could be implemented in the retrieval algorithm by realising parameters based on seasonal or monthly data, which of course would require a longer data record for a stable estimation. Also the so-called cross-ratio (CR) of VH- and VV-polarised backscatter images, which are usually recorded concurrently by S-1 in IW mode, bears much potential to account for vegetation signals, as documented recently [91]. Alternatively, vegetation data from optical satellite sensors could be used, once aggregated to e.g. 7- or 10-day averages to cope with the timing mismatch or data gaps because of cloud cover.

Despite these remaining issues, the 1km S-1 SSM demonstrated its capability to sense soil moisture at high spatio-temporal resolution, becoming especially valuable when changes in local hydrology due to rainfall or irrigation need to be captured. A recent study [92] found over Emilia-Romagna that the S-1 SSM product can quantify the impact of irrigation on local soil moisture, which is missed out by (downscaled) products from coarser sensors. This virtue of capturing small-scale changes is a clear difference to established (coarse-resolution) satellite products, thus the product constitutes a rich data source for agricultural and meteorological analysis and modelling.

Also, the prospect of the long-lasting Sentinel-1 mission attaches value on the S-1 SSM algorithm, facilitating a long and consistent data record on soil moisture at the comparatively high resolution of 1km, starting in 2015 and lasting at least until the end of 2030. While the data density is currently sufficient only over Europe and other selected areas, over time, the measurement number will reach serviceable levels all over the globe, fuelled since 2016 by two satellites in the orbit.

The Copernicus Global Land Service[8] (CGLS) of the European Commission disseminates operationally and freely soil moisture products together with other bio-geophysical variables to enable the monitoring of the global vegetation, water and energy budget. In recognition of the here presented findings, our method for retrieving 1km SSM from Sentinel-1 is currently in preparation towards operational product dissemination in the CGLS, featuring data in an initial phase over Europe, and subsequently globally.

ACKNOWLEDGMENTS

We would like to thank our colleagues from the TU Wien who supported us with the Sentinel-1 data management and processing, most notably Stefano Elefante and Le Tuan. We also thank the Italian Civil Protection Department for providing the rainfall maps.

REFERENCES

[1] M. Drusch, U. Del Bello, S. Carlier, O. Colin, V. Fernandez, F. Gascon, B. Hoersch, C. Isola, P. Laberinti, P. Martimort *et al.*, "Sentinel-2: ESA's optical high-resolution mission for GMES operational services," *Remote Sensing of Environment*, vol. 120, pp. 25–36, 2012.

[2] C. Donlon, B. Berruti, A. Buongiorno, M.-H. Ferreira, P. Féménias, J. Frerick, P. Goryl, U. Klein, H. Laur, C. Mavrocordatos *et al.*, "The global monitoring for environment and security GMES Sentinel-3 mission," *Remote Sensing of Environment*, vol. 120, pp. 37–57, 2012.

[3] R. Torres, P. Snoeij, D. Geudtner, D. Bibby, M. Davidson, E. Attema, P. Potin, B. Rommen, N. Floury, M. Brown *et al.*, "GMES Sentinel-1 mission."

[4] S. I. Seneviratne, T. Corti, E. L. Davin, M. Hirschi, E. B. Jaeger, I. Lehner, B. Orlowsky, and A. J. Teuling, "Investigating soil moisture–climate interactions in a changing climate: A review," *Earth-Science Reviews*, vol. 99, no. 3, pp. 125–161, 2010.

[5] C. M. Taylor, R. a. M. de Jeu, F. Guichard, P. P. Harris, and W. a. Dorigo, "Afternoon rain more likely over drier soils," *Nature*, vol. 489, no. 7416, pp. 423–426, Sep. 2012.

[6] D. R. Legates, R. Mahmood, D. F. Levia, T. L. DeLiberty, S. M. Quiring, C. Houser, and F. E. Nelson, "Soil moisture: A central and unifying theme in physical geography," *Progress in Physical Geography*, vol. 35, no. 1, pp. 65–86, Nov. 2011.

[7] S. I. Seneviratne, M. Wilhelm, T. Stanelle, B. Hurk, S. Hagemann, A. Berg, F. Cheruy, M. E. Higgins, A. Meier, V. Brovkin *et al.*, "Impact of soil moisture-climate feedbacks on CMIP5 projections: First results from the GLACE-CMIP5 experiment," *Geophysical Research Letters*, vol. 40, no. 19, pp. 5212–5217, 2013.

[8] R. D. Koster, P. a. Dirmeyer, Z. Guo, G. Bonan, E. Chan, P. Cox, C. T. Gordon, S. Kanae, E. Kowalczyk, D. Lawrence, P. Liu, C.-H. Lu, S. Malyshev, B. McAvaney, K. Mitchell, D. Mocko, T. Oki, K. Oleson, A. Pitman, Y. C. Sud, C. M. Taylor, D. Verseghy, R. Vasic, Y. Xue, and T. Yamada, "Regions of strong coupling between soil moisture and precipitation." *Science*, vol. 305, no. 5687, pp. 1138–40, Aug. 2004.

[9] B. Bisselink, E. Van Meijgaard, A. Dolman, and R. De Jeu, "Initializing a regional climate model with satellite-derived soil moisture," *Journal of Geophysical Research: Atmospheres*, vol. 116, no. D2, 2011.

[10] C. Albergel, G. Balsamo, P. de Rosnay, J. Muñoz Sabater, and S. Boussetta, "A bare ground evaporation revision in the ECMWF land-surface scheme: evaluation of its impact using ground soil moisture and satellite microwave data," *Hydrology and Earth System Sciences Discussions*, vol. 9, no. 5, pp. 6715–6752, May 2012.

[11] L. Brocca, L. Ciabatta, C. Massari, T. Moramarco, S. Hahn, S. Hasenauer, R. Kidd, W. Dorigo, W. Wagner, and V. Levizzani, "Soil as a natural rain gauge: Estimating global rainfall from satellite soil moisture data," *Journal of Geophysical Research: Atmospheres*, vol. 119, no. 9, pp. 5128–5141, 2014.

[12] L. Ciabatta, L. Brocca, C. Massari, T. Moramarco, S. Gabellani, S. Puca, and W. Wagner, "Rainfall-runoff modelling by using SM2RAIN-derived and state-of-the-art satellite rainfall products over Italy," *International Journal of Applied Earth Observation and Geoinformation*, vol. 48, pp. 163–173, 2016.

[13] Y. Tramblay, R. Bouaicha, L. Brocca, W. Dorigo, C. Bouvier, S. Camici, and E. Servat, "Estimation of antecedent wetness conditions for flood modelling in northern Morocco," *Hydrology and Earth System Sciences*, vol. 16, no. 11, p. 4375, 2012.

[14] N. Wanders, D. Karssenberg, A. d. Roo, S. De Jong, and M. Bierkens, "The suitability of remotely sensed soil moisture for improving operational flood forecasting," *Hydrology and Earth System Sciences*, vol. 18, no. 6, pp. 2343–2357, 2014.

[15] P. Laiolo, S. Gabellani, L. Campo, F. Silvestro, F. Delogu, R. Rudari, L. Pulvirenti, G. Boni, F. Fascetti, N. Pierdicca *et al.*, "Impact of different satellite soil moisture products on the predictions of a continuous distributed hydrological model," *International Journal of Applied Earth Observation and Geoinformation*, vol. 48, pp. 131–145, 2016.

[16] E. Sutanudjaja, L. Van Beek, S. De Jong, F. Van Geer, and M. Bierkens, "Calibrating a large-extent high-resolution coupled groundwater-land surface model using soil moisture and discharge data," *Water Resources Research*, vol. 50, no. 1, pp. 687–705, 2014.

[17] J. Qiu, Q. Gao, S. Wang, and Z. Su, "Comparison of temporal trends from multiple soil moisture data sets and precipitation: The implication of irrigation on regional soil moisture trend," *International Journal of Applied Earth Observation and Geoinformation*, vol. 48, pp. 17–27, 2016.

[18] D. G. Miralles, A. J. Teuling, C. C. Van Heerwaarden, and J. Vilà-guerau De Arellano, "Mega-heatwave temperatures due to combined soil desiccation and atmospheric heat accumulation," *Nature geoscience*, vol. 7, no. 5, p. 345, 2014.

[19] H. Carrão, S. Russo, G. Sepulcre-Canto, and P. Barbosa, "An empirical standardized soil moisture index for agricultural drought assessment from remotely sensed data," *International Journal of Applied Earth Observation and Geoinformation*, vol. 48, pp. 74–84, 2016.

[8] https://land.copernicus.eu/global/

[20] B. Bauer-Marschallinger, W. A. Dorigo, W. Wagner, and A. I. van Dijk, "How oceanic oscillation drives soil moisture variations over mainland Australia: An analysis of 32 years of satellite observations," *Journal of Climate*, vol. 26, no. 24, pp. 10 159–10 173, 2013.

[21] W. Dorigo, R. de Jeu, D. Chung, R. Parinussa, Y. Liu, W. Wagner, and D. Fernández-Prieto, "Evaluating global trends (1988–2010) in harmonized multi-satellite surface soil moisture," *Geophysical Research Letters*, vol. 39, no. 18, p. L18405, Sep. 2012.

[22] J. Blunden and D. S. Arndt, "State of the climate in 2011," *Bulletin of the American Meteorological Society*, vol. 93, no. 7, pp. S1–S282, 2012.

[23] R. de Jeu and W. Dorigo, "On the importance of satellite observed soil moisture," *International Journal of Applied Earth Observation and Geoinformation*, vol. 45, pp. 107–109, 2016.

[24] J. P. Walker, G. R. Willgoose, and J. D. Kalma, "In situ measurement of soil moisture: A comparison of techniques," *Journal of Hydrology*, vol. 293, no. 1, pp. 85–99, 2004.

[25] W. Wagner, S. Hahn, R. Kidd, T. Melzer, Z. Bartalis, S. Hasenauer, J. Figa-Saldaña, P. de Rosnay, A. Jann, S. Schneider *et al.*, "The ASCAT soil moisture product: A review of its specifications, validation results, and emerging applications," *Meteorologische Zeitschrift*, vol. 22, no. 1, pp. 5–33, 2013.

[26] L. Li, P. W. Gaiser, B.-C. Gao, R. M. Bevilacqua, T. J. Jackson, E. G. Njoku, C. Rudiger, J.-C. Calvet, and R. Bindlish, "WindSat global soil moisture retrieval and validation," *IEEE Transactions on Geoscience and Remote Sensing*, vol. 48, no. 5, pp. 2224–2241, 2010.

[27] Y. H. Kerr, P. Waldteufel, P. Richaume, J. P. Wigneron, P. Ferrazzoli, A. Mahmoodi, A. Al Bitar, F. Cabot, C. Gruhier, S. E. Juglea *et al.*, "The SMOS soil moisture retrieval algorithm," *IEEE Transactions on Geoscience and Remote Sensing*, vol. 50, no. 5, pp. 1384–1403, 2012.

[28] S. K. Chan, R. Bindlish, P. E. O'Neill, E. Njoku, T. Jackson, A. Colliander, F. Chen, M. Burgin, S. Dunbar, J. Piepmeier *et al.*, "Assessment of the SMAP passive soil moisture product," *IEEE Transactions on Geoscience and Remote Sensing*, vol. 54, no. 8, pp. 4994–5007, 2016.

[29] K. Miyaoka, A. Gruber, F. Ticconi, S. Hahn, W. Wagner, J. Figa-Saldaña, and C. Anderson, "Triple collocation analysis of soil moisture from Metop-A ASCAT and SMOS against JRA-55 and ERA-Interim," *IEEE Journal of Selected Topics in Applied Earth Observations and Remote Sensing*, vol. 10, no. 5, pp. 2274–2284, 2017.

[30] M. S. Burgin, A. Colliander, E. G. Njoku, S. K. Chan, F. Cabot, Y. H. Kerr, R. Bindlish, T. J. Jackson, D. Entekhabi, and S. H. Yueh, "A comparative study of the SMAP passive soil moisture product with existing satellite-based soil moisture products," *IEEE Transactions on Geoscience and Remote Sensing*, vol. 55, no. 5, pp. 2959–2971, 2017.

[31] Y. H. Kaheil, M. K. Gill, M. McKee, L. A. Bastidas, and E. Rosero, "Downscaling and assimilation of surface soil moisture using ground truth measurements," *IEEE Transactions on Geoscience and Remote Sensing*, vol. 46, no. 5, pp. 1375–1384, 2008.

[32] A. Gevaert, R. M. Parinussa, L. J. Renzullo, A. I. van Dijk, and R. A. de Jeu, "Spatio-temporal evaluation of resolution enhancement for passive microwave soil moisture and vegetation optical depth," *International Journal of Applied Earth Observation and Geoinformation*, vol. 45, pp. 235–244, 2016.

[33] N. N. Das, D. Entekhabi, S.-B. Kim, T. Jagdhuber, S. Dunbar, S. Yueh, A. Colliander, E. Lopez-baeza, and J. Martinez-Fernandez, "High-Resolution Enhanced Product based on SMAP Active-Passive Approach using Sentinel-1A and 1B SAR Data," in *IEEE International Geoscience and Remote Sensing Symposium (IGARSS)*, July 2017.

[34] N. E. Verhoest, M. J. van den Berg, B. Martens, H. Lievens, E. F. Wood, M. Pan, Y. H. Kerr, A. Al Bitar, S. K. Tomer, M. Drusch *et al.*, "Copula-based downscaling of coarse-scale soil moisture observations with implicit bias correction," *IEEE Transactions on Geoscience and Remote Sensing*, vol. 53, no. 6, pp. 3507–3521, 2015.

[35] S. K. Tomer, A. Al Bitar, M. Sekhar, M. Zribi, S. Bandyopadhyay, K. Sreelash, A. Sharma, S. Corgne, and Y. Kerr, "Retrieval and multi-scale validation of soil moisture from multi-temporal SAR data in a semi-arid tropical region," *Remote Sensing*, vol. 7, no. 6, pp. 8128–8153, 2015.

[36] W. Qu, H. Bogena, J. A. Huisman, J. Vanderborght, M. Schuh, E. Priesack, and H. Vereecken, "Predicting subgrid variability of soil water content from basic soil information," *Geophysical research letters*, vol. 42, no. 3, pp. 789–796, 2015.

[37] J. Peng, A. Loew, O. Merlin, and N. E. Verhoest, "A review of spatial downscaling of satellite remotely sensed soil moisture," *Reviews of Geophysics*, 2017.

[38] I. Woodhouse, *Introduction to microwave remote sensing*. CRC Press, 2006.

[39] S. Paloscia, S. Pettinato, E. Santi, C. Notarnicola, L. Pasolli, and A. Reppucci, "Soil moisture mapping using Sentinel-1 images: Algorithm and preliminary validation," *Remote Sensing of Environment*, vol. 134, pp. 234–248, 2013.

[40] M. Aubert, N. N. Baghdadi, M. Zribi, K. Ose, M. El Hajj, E. Vaudour, and E. Gonzalez-Sosa, "Toward an operational bare soil moisture mapping using TerraSAR-X data acquired over agricultural areas," *IEEE Journal of Selected Topics in Applied Earth Observations and Remote Sensing*, vol. 6, no. 2, pp. 900–916, 2013.

[41] M. El Hajj, N. Baghdadi, M. Zribi, and H. Bazzi, "Synergic Use of Sentinel-1 and Sentinel-2 Images for Operational Soil Moisture Mapping at High Spatial Resolution over Agricultural Areas," *Remote Sensing*, vol. 9, no. 12, p. 1292, 2017.

[42] C. Pathe and W. Wagner, "Using ENVISAT ASAR global mode data for surface soil moisture retrieval over Oklahoma, USA," *IEEE Transactions on Geoscience and Remote Sensing*, vol. 47, no. 2, pp. 468–480, 2009.

[43] A. Dostálová, M. Doubková, D. Sabel, B. Bauer-Marschallinger, and W. Wagner, "Seven Years of Advanced Synthetic Aperture Radar (ASAR) Global Monitoring (GM) of Surface Soil Moisture over Africa," *Remote Sensing*, vol. 6, no. 8, pp. 7683–7707, 2014.

[44] A. Loew, R. Ludwig, and W. Mauser, "Derivation of surface soil moisture from ENVISAT ASAR wide swath and image mode data in agricultural areas," *IEEE Transactions on Geoscience and Remote Sensing*, vol. 44, no. 4, pp. 889–899, 2006.

[45] ESA Sentinel-1 Team, *Sentinel-1 User Handbook*, P. Potin, Ed. European Space Agency, 2013, no. GMES-S1OP-EOPG-TN-13-0001.

[46] F. De Zan and A. M. Guarnieri, "TOPSAR: Terrain observation by progressive scans," *IEEE Transactions on Geoscience and Remote Sensing*, vol. 44, no. 9, pp. 2352–2360, 2006.

[47] W. Wagner, D. Sabel, M. Doubkova, A. Bartsch, and C. Pathe, "The potential of Sentinel-1 for monitoring soil moisture with a high spatial resolution at global scale," in *Symposium of Earth Observation and Water Cycle Science*, 2009.

[48] M. Hornacek, W. Wagner, D. Sabel, H.-L. Truong, P. Snoeij, T. Hahmann, E. Diedrich, and M. Doubková, "Potential for high resolution systematic global surface soil moisture retrieval via change detection using Sentinel-1," *IEEE Journal of Selected Topics in Applied Earth Observations and Remote Sensing*, vol. 5, no. 4, pp. 1303–1311, 2012.

[49] A. Gruber, W. Wagner, A. Hegyiova, F. Greifeneder, and S. Schlaffer, "Potential of Sentinel-1 for high-resolution soil moisture monitoring," in *Geoscience and Remote Sensing Symposium (IGARSS), 2013 IEEE International*. IEEE, 2013, pp. 4030–4033.

[50] M. El Hajj, N. Baghdadi, M. Zribi, G. Belaud, B. Cheviron, D. Courault, and F. Charron, "Soil moisture retrieval over irrigated grassland using X-band SAR data," *Remote Sensing of Environment*, vol. 176, pp. 202–218, 2016.

[51] N. Baghdadi, M. El Hajj, M. Zribi, and S. Bousbih, "Calibration of the Water Cloud Model at C-Band for Winter Crop Fields and Grasslands," *Remote Sensing*, vol. 9, no. 9, p. 969, 2017.

[52] D. Michelson, "ERS-I SAR backscattering coefficients from bare fields with different tillage row directions," *International Journal of Remote Sensing*, vol. 15, no. 13, pp. 2679–2685, 1994.

[53] G. Satalino, F. Mattia, M. W. Davidson, T. Le Toan, G. Pasquariello, and M. Borgeaud, "On current limits of soil moisture retrieval from ERS-SAR data," *IEEE Transactions on Geoscience and Remote Sensing*, vol. 40, no. 11, pp. 2438–2447, 2002.

[54] W. Wagner, C. Pathe, M. Doubkova, D. Sabel, A. Bartsch, S. Hasenauer, G. Blöschl, K. Scipal, J. Martínez-Fernández, and A. Löw, "Temporal Stability of Soil Moisture and Radar Backscatter Observed by the Advanced Synthetic Aperture Radar (ASAR)," *Sensors*, vol. 8, no. 2, pp. 1174–1197, Feb. 2008.

[55] Z. Bartalis, K. Scipal, and W. Wagner, "Azimuthal anisotropy of scatterometer measurements over land," *IEEE Transactions on Geoscience and Remote Sensing*, vol. 44, no. 8, pp. 2083–2092, Aug. 2006.

[56] P. Burt and E. Adelson, "The Laplacian pyramid as a compact image code," *IEEE Transactions on communications*, vol. 31, no. 4, pp. 532–540, 1983.

[57] ESA-ESRIN, "Sentinel High Level Opration Plan," ESA, Tech. Rep. COPE-S1OP-EOPG-PL-15-0020, 2017.

[58] V. Naeimi, K. Scipal, Z. Bartalis, S. Hasenauer, and W. Wagner, "An improved soil moisture retrieval algorithm for ERS and METOP scatterometer observations," *IEEE Transactions on Geoscience and Remote Sensing*, vol. 47, no. 7, pp. 1999–2013, 2009.

[59] S. C. Brown, S. Quegan, K. Morrison, J. C. Bennett, and G. Cookmartin, "High-resolution measurements of scattering in wheat canopies-Implications for crop parameter retrieval," *IEEE Transactions on Geoscience and Remote Sensing*, vol. 41, no. 7, pp. 1602–1610, 2003.

[60] M. Vreugdenhil, W. A. Dorigo, W. Wagner, R. A. de Jeu, S. Hahn, and M. J. van Marle, "Analyzing the vegetation parameterization in the TU-Wien ASCAT soil moisture retrieval," *IEEE Transactions on Geoscience and Remote Sensing*, vol. 54, no. 6, pp. 3513–3531, 2016.

[61] W. Wagner, G. Lemoine, and H. Rott, "A method for estimating soil moisture from ERS scatterometer and soil data," *Remote Sensing of Environment*, vol. 4257, no. 99, 1999.

[62] W. Wagner, J. Noll, M. Borgeaud, and H. Rott, "Monitoring soil moisture over the Canadian prairies with the ERS scatterometer," *IEEE Transactions on Geoscience and Remote Sensing*, vol. 37, no. 1, pp. 206–216, 1999.

[63] K. Scipal, M. Drusch, and W. Wagner, "Assimilation of a ERS scatterometer derived soil moisture index in the ECMWF numerical weather prediction system," *Advances in Water Resources*, vol. 31, no. 8, pp. 1101–1112, Aug. 2008.

[64] M. Doubková, A. I. Van Dijk, D. Sabel, W. Wagner, and G. Blöschl, "Evaluation of the predicted error of the soil moisture retrieval from C-band SAR by comparison against modelled soil moisture estimates over Australia," *Remote Sensing of Environment*, vol. 120, pp. 188–196, May 2012.

[65] V. Naeimi, Z. Bartalis, and W. Wagner, "ASCAT Soil Moisture: An Assessment of the Data Quality and Consistency with the ERS Scatterometer Heritage," *Journal of Hydrometeorology*, vol. 10, no. 2, pp. 555–563, Apr. 2009.

[66] L. Brocca, F. Melone, T. Moramarco, W. Wagner, and S. Hasenauer, "ASCAT soil wetness index validation through in situ and modeled soil moisture data in central Italy," *Remote Sensing of Environment*, vol. 114, no. 11, pp. 2745–2755, Nov. 2010.

[67] S. Schneider, Y. Wang, W. Wagner, and J.-F. Mahfouf, "Impact of ASCAT soil moisture assimilation on regional precipitation forecasts: A case study for Austria," *Monthly Weather Review*, vol. 142, no. 4, pp. 1525–1541, 2014.

[68] I. Mladenova, V. Lakshmi, J. P. Walker, R. Panciera, W. Wagner, and M. Doubkova, "Validation of the ASAR global monitoring mode soil moisture product using the NAFE'05 data set," *IEEE Transactions on Geoscience and Remote Sensing*, vol. 48, no. 6, pp. 2498–2508, 2010.

[69] B. Bauer-Marschallinger, S. Cao, S. Schaufler, C. Paulik, V. Naeimi, and W. Wagner, "1km Soil Moisture from Downsampled Sentinel-1 SAR Data: Harnessing Assets and Overcoming Obstacles," in *Geophysical Research Abstracts*, vol. Vol. 19.

[70] V. Naeimi, S. Elefante, S. Cao, W. Wagner, A. Dostalova, and B. Bauer-Marschallinger, "Geophysical parameters retrieval from Sentinel-1 SAR data: a case study for high performance computing at EODC," in *Proceedings of the 24th High Performance Computing Symposium*. Society for Computer Simulation International, 2016, p. 10.

[71] I. Ali, V. Naeimi, S. Cao, S. Elefante, B. Bauer-Marschallinger, and W. Wagner, "Sentinel-1 data cube exploitation: Tools, products, services and quality control," *Proc. Big Data Space*, pp. 40–43, 2017.

[72] B. Bauer-Marschallinger, D. Sabel, and W. Wagner, "Optimisation of global grids for high-resolution remote sensing data," *Computers & Geosciences*, vol. 72, 2014.

[73] T. Hengl, J. M. de Jesus, G. B. Heuvelink, M. R. Gonzalez, M. Kilibarda, A. Blagotić, W. Shangguan, M. N. Wright, X. Geng, B. Bauer-Marschallinger *et al.*, "SoilGrids250m: Global gridded soil information based on machine learning," *PLOS ONE*, vol. 12, no. 2, p. e0169748, 2017.

[74] G. Büttner, T. Soukup, and B. Kosztra, "CLC2012 addendum to CLC2006 technical guidelines," *Final Draft, Copenhagen (EEA)*, 2014.

[75] S. W. Smith, *The scientist and engineer's guide to digital signal processing*. California Technical Pub., 1999.

[76] W. Wagner, G. Lemoine, M. Borgeaud, and H. Rott, "A study of vegetation cover effects on ERS scatterometer data," *IEEE Transactions on Geoscience and Remote Sensing*, vol. 37, no. 2, pp. 938–948, 1999.

[77] L. Brocca, F. Melone, and T. Moramarco, "On the estimation of antecedent wetness conditions in rainfall–runoff modelling," *Hydrological Processes*, vol. 22, no. 5, pp. 629–642, 2008.

[78] L. Brocca, L. Ciabatta, T. Moramarco, F. Ponziani, N. Berni, and W. Wagner, "Use of satellite soil moisture products for the operational mitigation of landslides risk in central Italy," in *Satellite Soil Moisture Retrieval*. Elsevier, 2016, pp. 231–247.

[79] L. Brocca, S. Camici, F. Melone, T. Moramarco, J. Martínez-Fernández, J.-F. Didon-Lescot, and R. Morbidelli, "Improving the representation of soil moisture by using a semi-analytical infiltration model," *Hydrological Processes*, vol. 28, no. 4, pp. 2103–2115, 2014.

[80] L. Brocca, F. Melone, T. Moramarco, W. Wagner, V. Naeimi, Z. Bartalis, and S. Hasenauer, "Improving runoff prediction through the assimilation of the ASCAT soil moisture product," *Hydrology and Earth System Sciences*, vol. 14, no. 10, pp. 1881–1893, Oct. 2010.

[81] L. Brocca, S. Hasenauer, T. Lacava, F. Melone, T. Moramarco, W. Wagner, W. Dorigo, P. Matgen, J. Martínez-Fernández, P. Llorens, J. Latron, C. Martin, and M. Bittelli, "Soil moisture estimation through ASCAT and AMSR-E sensors: An intercomparison and validation study across Europe," *Remote Sensing of Environment*, vol. 115, no. 12, pp. 3390–3408, Dec. 2011.

[82] W. A. Dorigo, W. Wagner, R. Hohensinn, S. Hahn, C. Paulik, a. Xaver, a. Gruber, M. Drusch, S. Mecklenburg, P. van Oevelen, a. Robock, and T. Jackson, "The International Soil Moisture Network: A data hosting facility for global in situ soil moisture measurements," *Hydrology and Earth System Sciences*, vol. 15, no. 5, pp. 1675–1698, May 2011.

[83] C. Paulik, W. Dorigo, W. Wagner, and R. Kidd, "Validation of the ASCAT Soil Water Index using in situ data from the International Soil Moisture Network," *International Journal of Applied Earth Observation and Geoinformation*, vol. 30, pp. 1–8, 2014.

[84] W. Dorigo, A. Gruber, R. De Jeu, W. Wagner, T. Stacke, A. Loew, C. Albergel, L. Brocca, D. Chung, R. Parinussa *et al.*, "Evaluation of the ESA CCI soil moisture product using ground-based observations," *Remote Sensing of Environment*, vol. 162, pp. 380–395, 2015.

[85] Q. Wu, H. Liu, L. Wang, and C. Deng, "Evaluation of AMSR2 soil moisture products over the contiguous United States using in situ data from the International Soil Moisture Network," *International journal of applied earth observation and geoinformation*, vol. 45, pp. 187–199, 2016.

[86] M. Zreda, W. Shuttleworth, X. Zeng, C. Zweck, D. Desilets, T. Franz, and R. Rosolem, "COSMOS: the cosmic-ray soil moisture observing system," *Hydrology and Earth System Sciences*, vol. 16, no. 11, pp. 4079–4099, 2012.

[87] C. Albergel, P. de Rosnay, C. Gruhier, J. Muñoz Sabater, S. Hasenauer, L. Isaksen, Y. Kerr, and W. Wagner, "Evaluation of remotely sensed and modelled soil moisture products using global ground-based in situ observations," *Remote Sensing of Environment*, vol. 118, pp. 215–226, Mar. 2012.

[88] C. Massari, L. Brocca, A. Tarpanelli, and T. Moramarco, "Data assimilation of satellite soil moisture into rainfall-runoff modelling: A complex recipe?" *Remote Sensing*, vol. 7, no. 9, pp. 11 403–11 433, 2015.

[89] S. Schaufler, B. Bauer-Marschallinger, S. Hochstöger, and W. Wagner, "Modelling and Correcting Azimuthal Anisotropy in Sentinel-1 Backscatter Data," *Remote Sensing Letters*, in review.

[90] V. Naeimi, C. Paulik, A. Bartsch, W. Wagner, R. Kidd, S.-E. Park, K. Elger, and J. Boike, "ASCAT Surface State Flag (SSF): Extracting information on surface freeze/thaw conditions from backscatter data using an empirical threshold-analysis algorithm," *IEEE Transactions on Geoscience and Remote Sensing*, vol. 50, no. 7, pp. 2566–2582, 2012.

[91] A. Veloso, S. Mermoz, A. Bouvet, T. Le Toan, M. Planells, J.-F. Dejoux, and E. Ceschia, "Understanding the temporal behavior of crops using Sentinel-1 and Sentinel-2-like data for agricultural applications," *Remote Sensing of Environment*, vol. 199, pp. 415–426, 2017.

[92] L. Brocca, A. Tarpanelli, P. Filippucci, W. Dorigo, F. Zaussinger, A. Gruber, and D. F. Prieto, "How much water is used for irrigation? a new approach exploiting satellite soil moisture observations," in *EGU General Assembly 2018*, vol. Vol. 20, 2018, p. 4558, talk: European Geosciences Union, General Assembly 2018 (EGU 2018), Vienna; 2018-04-09 – 2018-04-13.

Bernhard Bauer-Marschallinger (M'18) received his master degree (MSc) in Geodesy and Geophysics from the TU Wien in 2012 and is currently pursuing the PhD degree in Remote Sensing.

As part of the TU Wien remote sensing research group, he has been involved in scientific and operational projects from ESA, EU FP7/H2020, Copernicus Global Land Services and Austrian Research Promotion Agency (FFG), mainly working on the development of SAR processing software and exploitation of satellite data, as well as on optimised spatial referencing of geodata. The retrieval of geophysical variables is in the focus of his research, aiming on the retrieval of soil moisture, vegetation health and water bodies. Most recently, he researches on the fusion of satellite observations from different spatial and temporal scales in order to obtain soil moisture information at high spatio-temporal resolution.

Vahid Freeman (formerly Naeimi) received the PhD degree in microwave remote sensing from the Vienna University of Technology (TU Wien), Vienna, Austria, in 2009. He has been working with the Institute of Photogrammetry and Remote Sensing, TU Wien, since 2005. From 2010 to 2013, he was with German Remote Sensing Data Centre at DLR. He is currently with the Department of Geodesy and Geoinformatiom at TU Wien.

His main research interests include geophysical parameters retrieval from remote sensing data especially active sensor (SAR and Scatterometers). He has participated in several national and international projects and actively involved in scientific algorithms development, prototyping, processing chains implementation, and high-performance computing.

Senmao Cao received his MSc degree in remote sensing of environment and resources from the Spatial Information Research Center of Fujian, Fuzhou University, China, in 2011. His master study focused on feature extraction and classification for remote sensing imagery, specializing in semi-supervised learning.

From 2011 to 2013, he worked for Beijing Earth-View Image, Inc., as a Software Developer, where he was responsible for the development of remote sensing image processing tools, GIS database design, and performance optimization. Since May 2014, he has been with the Department of Geodesy and Geoinformation at TU Wien, concentrating on the development of SAR processing chain. His research interests include soil moisture retrieval, flood mapping, and scientific programming. He specializes in image processing, scientific programming, and data analysis computing.

Christoph Paulik has worked in the field of radar remote sensing since 2010. He has done research in soil moisture and freeze/thaw state retrieval and their validation while also building operational processing chains for the Copernicus Global Land and Climate Change services. He is now part of VanderSat's operations team.

Stefan Schaufler was born in Braunau am Inn, Austria, in 1988. He received his MSc degree in Geodesy and Geomatics Engineering with excellence from TU Wien in 2016.

From 2016 to 2017, he worked as project assistant at the Department of Geodesy and Geoinformation at TU Wien. Since 2017 he is working as a GNSS product engineer in the GNSS Product Management group at Leica Geosystems. His research interests are signal processing, identifying patterns in time series data and sensor fusion.

Tobias Stachl was born in Braunau/Inn, Austria, in 1994. He is currently studying Geodesy and Geoinformatics at TU Wien, and working towards his BSc degree. He has been a project assistant since November 2017 at the Department of Geodesy and Geoinformation at TU Wien.

His main interests are automated global-scale data processing and research in the retrieval of probabilities of frozen soil and scaling issues from SAR data.

Sara Modanesi was born in Tarquinia, Italy, in 1985. She received a MSc degree in Applied Geology in 2012 and a Master degree in Analysis and Management of Hydrological Hazard in 2016, from Sapienza University (Rome), both with excellence.

Currently she is working with a research scholarship at the Research Institute of Geo-Hydrological Protection (IRPI) of the National Research Council (CNR) in Perugia, Italy. Her main research interest is the validation and application of innovative satellite products for the improvement of hydrological modelling and drought monitoring.

Christian Massari was born was born in Cascia, Italy, in 1981. He received the MSc degree in environmental engineering and the PhD degree in hydraulic engineering, both with excellence, from the University of Perugia, Italy, in 2008 and 2012, respectively. He received fellowships to carry out research at the Department of Hydrology and Water Resources, University of Arizona, Tucson, USA, where he has worked in the field of hydraulic groundwater and hydraulic tomographic techniques. From 2011 to 2013, he has been a Research Fellow with the Dipartimento di Ingegneria Civile ed Ambientale, University of Perugia, where he has worked in the development of data fusion techniques for the diagnosis of pressurized pipe systems. From 2013 to 2016 he has been postdoctoral researcher with the Research Institute for Geo- Hydrological Protection, National Research Council (CNR), Perugia, Italy, where he has been working in the field of hydrology, remote sensing and data assimilation. During spring 2016 he has been visiting scientist at the US Department of Agriculture (USDA) in Beltsville, USA, where he has worked in the error characterization of satellite precipitation products. From January 2017 he is permanent researcher of the CNR.

His research interests include data fusion and data assimilation of hydrological variables (e.g., soil moisture and rainfall), hydro-validation of satellite soil moisture and rainfall observations, filtering of satellite soil moisture, flooding risk analysis, and flood frequency assessment. He is member of SII, GII, EGU, and AGU.

Luca Ciabatta was born in Perugia, Italy, in 1985. He received the MSc degree in Geological Sciences and Technologies with excellence, from the University of Perugia in 2012. Since 2014, he is a research fellow at the Research Institute of Geo-Hydrological Protection (IRPI) of the National Research Council (CNR) of Perugia.

His research interests mainly regard the use of satellite data for hydrological applications and natural hazards mitigation. He is involved in satellite data validation activities, in the development of satellite-derived rainfall datasets and in the development of hydrological models. He is currently undertaking his PhD in Civil and Environmental Engineering jointly at the University of Florence and at TU Wien. He is member of GII and EGU.

Luca Brocca was born in Genoa, Italy, in 1978. He received the MSc degree in Environmental Engineering and the PhD degree in Civil Engineering, both with excellence, from the University of Perugia, Italy, in 2003 and 2008, respectively.

Since 2009 he is a researcher at the Research Institute of geo-Hydrological Protection (IRPI) of the National Research Council (CNR) in Perugia, Italy. He has been author and co-author of 107 journal papers and 76 papers in conference proceedings with 4000+ citations. He serves as reviewer for ¿35 international journals and as Associate Editor for Geoderma and Hydrology journals. He actively participates to several research project in the frame of Italian and European programs (LIFE+, HORIZON2020), and funded by Space Agencies (ESA, EUMETSAT), in collaboration with Italian and international institutions. He is involved in teaching and tutorial activity for the University of Perugia.

The main research interest is the development innovative methods for exploiting satellite observations (soil moisture, rainfall, discharge) in hydrological applications (flood, landslide, drought, etc). He is the Italian National Correspondent of the Euromediterranean network of Experimental and Representative Basins (ERB) and he is member of IAHS, SII, GII, iEMSs, and EGU.

Wolfgang Wagner (M'98–SM'07) was borne in Austria in 1969. He received the Dipl.-Ing. degree in physics and the Dr.techn. degree in remote sensing from the TU Wien, Austria, in 1995 and 1999 respectively.

In support of his master and PhD studies he received fellowships to carry out research at NASA, ESA, and the EC Joint Research Centre. From 1999 to 2001 he was with DLR. In 2001 he was appointed professor for remote sensing at TU Wien. Since 2012 he has been head of the Department of Geodesy and Geoinformation of TU Wien. He is co-founder and senior scientist at the EODC Earth Observation Data Centre. His main research interest is to gain physical understanding of the mechanisms driving the interaction of electromagnetic waves with the land surface. He has developed models for retrieving soil moisture, biomass, and other land surface variables from scatterometer, SAR and full-waveform lidar observations. He is member of the EUMETSAT/ESA Science Advisory Group for METOP-SG SCA, and since 2016 chair of the GCOS/WCRP Terrestrial Observation Panel for Climate. From 2008 to 2012 he served as ISPRS Commission VII President and from 2009-2011 as editor-in-chief of the Open Access Journal "Remote Sensing". He is a recipient of the ISPRS Frederick J. Doyle Award for his scientific contributions in active remote sensing.